



HAL
open science

Brain white matter oedema due to CIC-2 chloride channel deficiency: an observational analytical study.

Christel Depienne, Marianna Bugiani, Céline Dupuits, Damien Galanaud, Valérie Touitou, Nienke Postma, Carola van Berkel, Emiel Polder, Eleonore Tollard, Frédéric Darios, et al.

► **To cite this version:**

Christel Depienne, Marianna Bugiani, Céline Dupuits, Damien Galanaud, Valérie Touitou, et al.. Brain white matter oedema due to CIC-2 chloride channel deficiency: an observational analytical study.. *The Lancet Neurology*, 2013, 12 (7), pp.659-68. 10.1016/S1474-4422(13)70053-X . inserm-00842764

HAL Id: inserm-00842764

<https://inserm.hal.science/inserm-00842764>

Submitted on 22 Nov 2013

HAL is a multi-disciplinary open access archive for the deposit and dissemination of scientific research documents, whether they are published or not. The documents may come from teaching and research institutions in France or abroad, or from public or private research centers.

L'archive ouverte pluridisciplinaire **HAL**, est destinée au dépôt et à la diffusion de documents scientifiques de niveau recherche, publiés ou non, émanant des établissements d'enseignement et de recherche français ou étrangers, des laboratoires publics ou privés.

Brain white matter oedema due to CIC-2 chloride channel deficiency: an observational analytical study

Christel Depienne PhD,* Marianna Bugiani MD,* Céline Dupuits MSc, Prof. Damien Galanaud MD, Valérie Touitou MD, Nienke Postma, Carola van Berkel, Emiel Polder, Eleonore Tollard MD, Frédéric Darios PhD, Prof. Alexis Brice MD, Prof. Christine E. de Die-Smulders MD, Prof. Johannes S. Vles MD, Adeline Vanderver MD, Graziella Uziel MD, Prof. Cengiz Yalcinkaya MD, Suzanna G. Frints MD, Vera M. Kalscheuer PhD, Jan Klooster MSc, Prof. Maarten Kamermans PhD, Truus E.M. Abbink PhD, Nicole I. Wolf MD, Frédéric Sedel MD,** Prof. Marjo S. van der Knaap MD**

INSERM, U975 - CRICM, Hôpital Pitié-Salpêtrière, 75 013 Paris, France (C Depienne, F. Darios, A Brice); **Université Pierre et Marie Curie-Paris-6 (UPMC), 75 013 Paris, France** (C Depienne, D Galanaud, F Darios, A Brice, F Sedel); **AP-HP, Hôpital Pitié-Salpêtrière, Département de Génétique et de Cytogénétique, 75 013 Paris, France** (C Depienne, A Brice), **AP-HP, Hôpital Pitié-Salpêtrière, Unité Fonctionnelle Neurométabolique, 75 013 Paris, France** (C Depienne, C Dupuits, F Sedel); **AP-HP, Hôpital Pitié-Salpêtrière, Service de Neuroradiologie, 75 013 Paris, France** (D Galanaud); **AP-HP, Hôpital Pitié-Salpêtrière, Service d'Ophthalmologie, 75 013 Paris, France** (V Touitou); **CHU de Rouen, Service de Radiologie, 76 000 Rouen, France** (E Tollard); **AP-HP, Hôpital Pitié-Salpêtrière, Département de Neurologie, 75 013 Paris, France** (F Sedel); **Departments of Clinical Genetics (C E de Die-Smulders, S G Frints) and Child Neurology (J S Vles), Maastricht University Medical Center, Maastricht, the Netherlands**; **Department of Neurology, Children's National Medical Center, Washington, USA** (A Vanderver); **Unit of Child Neurology, "Carlo Besta" Neurological Institute Foundation, Milan, Italy** (G Uziel); **Division of Child Neurology, Neurology Department, Cerrahpasa Medical School, Istanbul University (C Yalcinkaya)**; **Max Planck Institute for Molecular Genetics, Department Human Molecular Genetics, Berlin, Germany** (V M Kalscheuer); **Department of Retinal Signal Processing, Netherlands Institute for Neuroscience-KNAW, Amsterdam, the Netherlands** (J Klooster, M Kamermans); **Department of Neurogenetics, Academic Medical Center, Amsterdam, the Netherlands** (M Kamermans); **Departments of Pathology (M Bugiani) and Child Neurology (M Bugiani, N Postma, C van Berkel, E Polder, T E M Abbink, N I Wolf, M S van der Knaap), Neuroscience Campus Amsterdam and VU University Medical Center, Amsterdam, the Netherlands.**

* Authors contributed equally

** Co-last authors

Correspondence to:

Dr. Christel Depienne at INSERM, U975 - CRICM, Hôpital Pitié-Salpêtrière, 47-83 boulevard de l'Hôpital, 75 013 Paris, France

christel.depienne@upmc.fr

or Prof. Marjo Van der Knaap, at Department of Child Neurology, VU University Medical Center, De Boelelaan 1117, 1081 HV Amsterdam, The Netherlands

ms.vanderknaap@vumc.nl

Summary

Background The function of chloride channel CIC-2 in human physiology is under debate. Controversial studies in patients have suggested a role in idiopathic epilepsies, whereas mutant mouse models indicate functions in ion and water homeostasis.

Methods We used exome sequencing to identify the gene involved in a novel leukoencephalopathy characterized by MRI signal abnormalities in the posterior limbs of the internal capsules, midbrain cerebral peduncles and middle cerebellar peduncles. The candidate gene was screened in additional patients by Sanger sequencing and mRNA analysis. The functional consequences of the mutations were investigated. The localization of CIC-2 was assessed by immunohistochemistry and electron microscopy in postmortem human brains.

Findings We identified homozygous or compound-heterozygous mutations in *CLCN2*, encoding CIC-2, in three adult and three pediatric patients. The *CLCN2* mutations resulted in loss-of-function of CIC-2. One pediatric patient with the same MRI abnormalities and X-linked family history had a mutation in *GJB1*, encoding connexin32. Clinical features were variable and included cerebellar ataxia, spasticity, chorioretinopathy with visual field defects, optic neuropathy, cognitive defects and headaches. MRIs showed restricted diffusion suggesting myelin vacuolation, in adult patients limited to the specified white matter structures, in pediatric patients more diffusely involving white matter. We found CIC-2 in all components of the panglial syncytium, enriched in astrocytic endfeet at the perivascular basal lamina and glia limitans and in ependymal cells.

Interpretation Our observations substantiate the concept that CIC-2 is involved in brain ion and water homeostasis. Autosomal-recessive *CLCN2* mutations cause a leukoencephalopathy that belongs to an emerging group of disorders, one of which is megalencephalic leukoencephalopathy with subcortical cysts, affecting brain ion and water homeostasis and characterized by intramyelinic edema.

Funding ELA association, INSERM and AP-HP (PHRC n°AOM 10300), the Dutch Organisation for Scientific Research (ZonMw, TOP grants 903-42-097 and 9120.6002 and VENI grant 016.066.017), E-Rare (grant 11-330-1024), the Hersenstichting (grant 2009(2)-14), the Optimix Foundation for Scientific Research, the Myelin Disorders Bioregistry Project, NINDS K08NS060695, and Project GENCODYS (241995, funded by the European Union Framework Programme 7).

Introduction

CIC-2 is a chloride channel that is almost ubiquitously expressed in the human body.¹ It is present in plasma membranes and is activated by hyperpolarization, acidic extracellular pH, and osmotic cell swelling.¹⁻⁴ Its functions in human physiology are a matter of debate. Roles in gastric acid secretion, lung development and function, and nephronogenesis have been suggested, but not confirmed.^{1,5} Information on the localization of CIC-2 within the brain comes from rodent studies, where it has been noted in oligodendrocytes, astrocytes (especially in endfeet), and pyramidal and non-pyramidal neurons in the hippocampus.^{6,7} There is evidence that CIC-2 modulates postsynaptic responses to GABA by influencing intracellular chloride concentration in neurons⁸ or regulates neuronal excitability,^{9,10} but the physiological relevance of these findings has not been confirmed.

Physiological roles of proteins can be gleaned from diseases caused by mutations in their genes. No human disease has been unequivocally related to mutations in *CLCN2*, the gene encoding CIC-2. Heterozygous mutations were described as a cause of idiopathic generalized epilepsies,¹¹⁻¹⁸ but this was later refuted^{1,19} and the original paper¹¹ had to be withdrawn.¹⁸ Mutant mice lacking functional CIC-2 display blindness due to photoreceptor degeneration and leukoencephalopathy with intramyelinic edema.^{5,6,20} Based on the latter finding, it was proposed that CIC-2 is involved in brain ion and water homeostasis,^{5,6} but confirmatory human data have been lacking until now. A known human disorder characterized by intramyelinic edema is megalencephalic leukoencephalopathy with subcortical cysts (MLC).²¹⁻²³ Mutations in *MLC1* are identified in 75% of MLC patients.^{24,25} No mutations in *CLCN2* were found in the *MLC1*-negative patients.²⁶ Recently, mutations in *GLIALCAM* were identified in those patients.²⁷ Interestingly, GlialCAM is a putative auxiliary subunit of both CIC-2 and *MLC1*.^{27,28}

In the present paper we present a human disease related to *CLCN2* mutations and provide evidence that CIC-2 is involved in brain water and ion homeostasis.

Methods

The study was performed with approval of the Institutional Review Boards and informed consent of patients and families.

MRI

We study magnetic resonance imaging (MRI) of patients with leukoencephalopathies of unknown origin with the aim to define novel disorders by distinct patterns of MRI abnormalities.²⁹ We score appearance and distribution of signal abnormalities. We assess apparent diffusion coefficient (ADC) values in areas of abnormal signal. Signal intensity on T₂- and T₁-weighted images and ADC values provide information on tissue micro-structure. High ADC values indicate large water spaces; low ADC values indicate small water spaces. The study is multi-institutional and MRIs have been made with different pulse sequences on machines of different vendors. For this reason, we use a robust cut-off ADC value of 60 10⁻⁵ mm²/s, below which the diffusion is considered restricted. Subtle diffusion restriction may, therefore, be missed.

We observed several patients with prominent signal abnormalities in the middle cerebellar peduncles, midbrain cerebral peduncles and posterior limbs of the internal capsules and used these features as inclusion criteria for the present study. We found this MRI pattern in three patients with adult-onset disease and four patients with childhood-onset disease.

Exome and Sanger sequencing

Exome sequencing was performed in the three patients with adult onset disease (Appendix). A single pediatric patient came from a family with X-linked disease inheritance. This family participated in another exome sequencing study focused on X-linked disorders.

The *CLCN2* gene was sequenced in the adult and pediatric patients; *GJB1*, encoding connexin32 (Cx32), was sequenced in *CLCN2*-negative male patients (Appendix).

Functional studies

CLCN2 mRNA was quantified in fibroblasts of adult patients with *CLCN2* mutations. Transient transfections of wild-type or mutant CIC-2-V5-His6 expression plasmids in Cos7 cells were used to study the functional consequences of *CLCN2* mutations (Appendix).

Immunohistochemistry and electron microscopy

To define which cell types express CIC-2 in normal mature human brain, we examined the posterior limb of the internal capsule, frontal white matter, frontal cortex and ependyma by fluorescence immunohistochemistry. Tissue was obtained at autopsy from nine control subjects aged 1-75 years (Appendix), who succumbed to heart disease or extra-cerebral neoplasm. None of the subjects had neurological symptoms. Neuropathologic examination showed no abnormalities.

Immunohistochemistry (Appendix) was performed on frozen tissue using antibodies against CIC-2, GlialCAM and MLC1, as well as glial fibrillary acidic protein (GFAP, astrocyte marker), oligodendrocyte transcription factor-2 (olig2, oligodendrocyte marker), neuronal nuclear antigen (NeuN, neuronal marker), platelet endothelial cell adhesion molecule-1 (PECAM1/CD31, endothelial marker), and phosphorylated and non-phosphorylated neurofilament H (SMI31 and SMI32, respectively, axonal markers). The anti-CIC-2 antibodies were validated for specificity (Appendix, Figures S5 and S6). All sections were counterstained with DAPI (nuclear staining).

Electron microscopy (Appendix) was performed on tissue from the posterior limb of the internal capsule. Sections were incubated with CIC-2, GlialCAM and MLC1 antibodies.

Role of the funding sources

The sponsors of the study had no role in study design, data collection, data analysis, data interpretation, or writing of the report. The corresponding authors had full access to all the data in the study and had final responsibility for the decision to submit for publication.

Results

Patients

The three patients with adult-onset disease were unrelated (patients 1-3, Table S1, Figure S1). They had mild cerebellar ataxia and a variable combination of chorioretinopathy with visual field defects, optic neuropathy and headaches. One patient had a schizophrenia-like disorder. The three patients with childhood-onset disease and *CLCN2* mutations (patients 4-6, Table S1) had mild cerebellar ataxia and a variable combination of mild spasticity, visual field defects, learning disabilities and headaches.

The patient with X-linked disease (patient 7, Table S1; Figure S1) presented with nystagmus at 12 months. He developed incapacitating cerebellar ataxia and spasticity. There was no clinical evidence of peripheral nerve involvement, although recent neurophysiological investigations revealed mild motor neuropathy. Affected male family members had the same clinical and MRI findings. Carrier females had no complaints.

MRI

All patients had prominent signal abnormalities and decreased ADC values in the posterior limbs of the internal capsules, cerebral peduncles in the midbrain, pyramidal tracts in the pons and middle cerebellar peduncles (Figure 1, Table S2).

All patients with adult-onset disease had additional signal abnormalities in specific brainstem tracts and the cerebellar white matter (Table S2). Cerebral hemispheric white matter abnormalities were mild and nonspecific. In one patient, low to borderline-low ADC values were also found in cerebral white matter areas.

In the pediatric patients, the same additional signal abnormalities in specific brainstem tracts and cerebellum were found. In addition, they had diffuse mild signal abnormality of the brain white matter, which was hyperintense relative to gray matter on both T₂- and T₁-weighted images (Figure 1, Table S2). Low to borderline-low ADC values were present in the cerebral and cerebellar hemispheric white matter and corpus callosum. The signal behavior of the white matter on T₁- and T₂-weighted images would suggest hypomyelination,³⁰ but hypomyelination is associated with increased size of water spaces and therefore increased ADC values.³¹ The low white matter ADC suggests myelin microvacuolation instead of hypomyelination.³² Increased intramyelinic water accounts for the mild T₂-signal changes.

CLCN2 and *GJB1* mutations

Assuming a single disease with autosomal recessive inheritance, we sequenced the entire exome of the adult patients (Tables S3 and S4). In patient 3, who has consanguineous parents, we determined homozygous regions (Table S5), in which we searched for homozygous mutations. We found 10 single nucleotide substitutions and two insertion-deletions with a possible impact on gene or protein function and absent from control databases (Table S6). One was a homozygous in-frame deletion (p.Leu144_Ile145del) in *CLCN2*. Analysis of exome data in the other adult patients revealed the same homozygous nonsense mutation (p.Trp570*) in *CLCN2* (Table 1, Figure S2). *CLCN2* was the only gene, common to the 3 adult patients, containing at least one homozygous or at least two heterozygous, possibly deleterious variants that were absent from exome data of individuals with other diseases analyzed at the same time (Table S7).

We then analyzed the coding sequence of *CLCN2* by Sanger sequencing in the pediatric patients. Homozygous or compound-heterozygous *CLCN2* mutations were identified in three (Table 1, Figure S2). All mutations were predicted to be pathogenic and

none were present in healthy controls of the same origin or in the Hapmap and 1000 genomes databases (Table S8).

Sequencing of the exome of the *CLCN2*-negative patient who had an X-linked family history revealed a novel missense mutation (p.Pro174Ser) in *GJB1* (Tables 1 and S8). This mutation was confirmed in his mother and in the single living affected male family member. In the remaining male patients, no mutations were found.

Functional consequences of *CLCN2* mutations

Quantification of the *CLCN2* mRNA in fibroblasts from patients and controls by real-time quantitative PCR showed that the mRNA with the p.Trp570* mutation was significantly down-regulated as compared to controls, contrary to the mRNA with p.Leu144_Ile145del (Figure S3). Treatment with emetin, an inhibitor of nonsense-mediated decay, rescued the mRNA expression, indicating that Trp570* leads to degradation of the mutant mRNA, although a substantial fraction of the mRNA subsists. We could not confirm presence of the truncated protein because expression of CIC-2 was undetectable in fibroblasts. Transient expression of the protein with the p.Trp570* mutation in Cos7 cells showed that the truncated protein, if expressed, has an aberrant localization restricted to the Golgi apparatus (Figure S4).

The p.Leu144_Ile145del and p.Ala500Val mutations affect conserved hydrophobic amino acids located in transmembrane domains of CIC-2, possibly leading to protein misfolding or misinsertion in the membrane. To test this hypothesis, we compared the expression and subcellular localization of V5-His6-tagged CIC-2 with the p.Leu144_Ile145del or p.Ala500Val mutation to those of the wild-type protein in Cos7 cells. Localization of the CIC-2-p.Leu144_Ile145del and p.Ala500Val proteins was restricted to the endoplasmic reticulum, whereas wild-type CIC-2 was present in different subcellular compartments including the plasma membrane (Figure 2A). In addition, the amount of both mutated CIC-2 proteins transiently expressed in Cos7 cells was lower than the wild-type form (Figure 2B) and they hardly reached the plasma membrane (Figure 2C). These findings indicate that CIC-2-p.Leu144_Ile145del and p.Ala500Val are trapped and degraded in the endoplasmic reticulum.

Altogether, these results show that all mutations identified in the patients lead to a complete or at least partial loss-of-function of the CIC-2 channel by different mechanisms.

Immunohistochemistry and electron microscopy

Immunohistochemistry revealed that virtually all GFAP⁺ fibrous astrocytes in the posterior limb of the internal capsule and frontal white matter express CIC-2 on the surface of both cell body and processes (Figure 3A). CIC-2 immunopositivity had a fine punctate quality (Figure 3A, inset), as expected for a membrane protein. Numerous CIC-2⁺ astrocytic processes ran parallel and perpendicular to axonal bundles (Figure 3A) and abutting axons (Figure S7). CIC-2 was enriched in perivascular astrocytes (Figure 3B), where GlialCAM (Figures 3C and S8A) and MLC1 (Figure S8B) were also expressed. GlialCAM and MLC1 immunoreactivity overlapped consistently and extended further distally than CIC-2 into astrocytic endfeet approaching the basal lamina (Figures 3C and S8A-B). A more discrete, punctate CIC-2 immunoreactivity was visible in an intermittent fashion along axons (Figure S7). Numerous CIC-2⁺/GFAP⁻ cells with the morphology of oligodendrocytes were observed. In the frontal cortex, CIC-2 expression was detected only in scattered protoplasmic astrocytes around blood vessels and in astrocytes that partake in the glia limitans (Figures 3D and S8C). In these locations, CIC-2⁺ astrocytes co-expressed GlialCAM (Figures 3E and S8C) and MLC1 (Figure S8D). No CIC-2 expression was found

in neuronal perikarya (Figure 3G). CIC-2 expression was also observed in the ependymal lining, again overlapping with GlialCAM (Figures 3G and S8E) and MLC1 (Figure S8F).

EM confirmed that CIC-2 was abundantly present in white matter astrocytes and enriched in cell processes contacting abaxonal myelin (Figure 4A) and contacting each other (Figure 4B). At these sites, GlialCAM showed a similar distribution (Figure 4C and D). CIC-2 immunoreactivity was also visible inside axons and at the axonal surface contacting adaxonal myelin (Figure S7). By contrast, GlialCAM and MLC1 were not detected in axons or myelin (Figure 4C). Around blood vessels, CIC-2 was found at astrocyte-astrocyte contacts in endfeet (Figure 4B), a site where also GlialCAM (Figure 4D) and MLC1 (Figure 4E) were present.

Discussion

In 2003, heterozygous mutations in *CLCN2* were reported as a cause of the most common forms of idiopathic generalized epilepsy, including childhood absence epilepsy, juvenile myoclonic epilepsy, and epilepsy with grand mal seizures on awakening.¹¹ Subsequent publications, however, identified *CLCN2* mutations in only a small proportion of such patients.¹²⁻¹⁶ The 2003 paper had to be retracted in 2009¹⁸, although the authors still believed that *CLCN2* mutations may contribute to epilepsy in some cases,^{17,18} which was vehemently debated by others.^{1,19} Functional studies of CIC-2 variants identified in patients with epilepsy did not confirm their pathogenicity and similar variants were observed in individuals without epilepsy.^{1,19} Our observations also do not support the hypothesis that loss-of-function mutations in *CLCN2* confer an increased risk of epilepsy. None of the six patients with homozygous or compound heterozygous mutations in *CLCN2* had epilepsy or a family history of epilepsy, indicating that partial or complete CIC-2 loss of function *per se* is insufficient to cause epilepsy.

We demonstrate that autosomal recessive loss-of-function mutations in *CLCN2* cause a leukoencephalopathy with MRI evidence of myelin micro-vacuolation. These findings are similar to those in CIC-2 deficient mice and in conformity with the concept that CIC-2 in the brain is involved in ion and water homeostasis.^{5,6}

The disease related to *CLCN2* mutations is variable in age of onset and clinical presentation. Mild cerebellar ataxia is the most consistent finding. Retinopathy, as found in the CIC-2 deficient mice, is observed in only part of the patients, although the visual field defects in absence of other ophthalmologic findings suggest that these patients may have a retinopathy that is too subtle to be picked up at funduscopy. CIC-2 deficient mice are sterile due to testicular degeneration. The adult patients in this paper are female. The only male patient does not show signs of testicular degeneration as a teenager. The clinical presentation of the patients is nonspecific and does not allow a diagnosis. However, the MRI findings are highly specific and allow a diagnosis. We have analyzed the *CLCN2* gene in several other adult and pediatric patients, who had MRI findings reminiscent of those of the present patients, but did not meet the MRI criteria as specified in the Methods; we did not find *CLCN2* mutations in any of them.

The phenotypic variability observed in the patients may at least in part be related to the degree of CIC-2 loss of function. The mutational spectrum and functional analyses both indicate loss-of-function of CIC-2, but it is possible that some mutated proteins, in particular C-terminally truncated or missense mutants that reach the plasma membrane in significant amounts, retain a partial function.

The present study adds to the growing insight into how the brain deals with the continuous shifts of ions and water related to action potentials. Brain white matter mainly consists of myelinated axons and its most important physiological function is impulse conduction. Action potentials are based on shifts in ions, which are obligatorily associated with osmotically driven shifts in water, requiring rapid compensation. Any disturbance of the compensatory mechanisms may disrupt impulse transmission or lead to life threatening changes in brain volume. Brain ion and water homeostasis is complex and involves electrolytes and organic osmolytes, channels and transporters, and coordinated processes like regulatory volume decrease and increase to correct cell volume changes.^{33,34} Astrocytes are central in this process. They are the most abundant and best connected cell type of the so-called “panglial syncytium”, a vast network of astrocytes, oligodendrocytes and ependymal cells interconnected by gap junctions. The panglial syncytium is essential for long-distance disposal of ions and water.^{33,34}

Action potentials are associated with the requirement of disposal of sub- and intramyelinic potassium.³⁴ In myelinated axons, depolarization is associated with influx of sodium at nodes of Ranvier; compensatory potassium efflux occurs in paranodal regions covered by myelin (Figure S9). Gap junctions facilitate transport of potassium and osmotic water across myelin layers into astrocytes. Cx32 constitutes gap junctions in paranodal myelin; Cx32 and connexin47 constitute gap junctions between myelin and astrocytes. The astrocytic syncytium allows rapid dispersion of potassium and buffers the associated volume changes. This process of so-called “potassium siphoning” prevents action potential-induced osmotic intramyelinic edema.³⁴ Disruptions of molecular components of these ion and water homeostatic pathways are associated with intramyelinic edema in human diseases and mutant mouse models.^{6,20,34-36} Interestingly, no myelin vacuolation occurs in mouse models in the absence of action potentials,^{6,35} confirming that it is mainly hindrance of compensation of action potential-induced ion and water shifts that leads to osmotic intramyelinic edema.

Insight into the mechanisms and molecular components of brain ion and water homeostatic pathways is still incomplete. Our study provides evidence that CIC-2 is one of these molecular components. The first observation supporting a role of CIC-2 in brain ion and water homeostasis is the MRI evidence of myelin micro-vacuolation in patients with *CLCN2* mutations. The second observation is the presence of the same MRI abnormalities with evidence of myelin micro-vacuolation in a patient with a *GJB1* mutation. Mutations in *GJB1*, encoding Cx32, lead to X-linked Charcot-Marie-Tooth (CMTX). In addition to peripheral neuropathy, CMTX patients may experience episodes of brain dysfunction with MRI evidence of transient myelin vacuolation.³⁷ We have no explanation why the mutation found in our family has a persistent effect on brain myelin, without any fluctuation, both clinically and on serial MRI. The serious spasticity and cerebellar ataxia probably overshadows the neuropathy, which was only found at neurophysiological studies after the *GJB1* mutation had been found. Other CMTX cases with persistent clinical signs of brain dysfunction and white matter disease on MRI have been reported, but diffusion findings were not mentioned.³⁸ The third observation supporting that the principal role of CIC-2 is in brain ion and water homeostasis is the CIC-2 membrane expression in the pial syncytium, with enhanced expression around blood vessels, in the glia limitans, ependymal lining, and astrocyte-astrocyte contacts in the white matter. The fourth observation is the finding that CIC-2 colocalizes with MLC1 and GlialCAM in astrocytic endfeet at the perivascular basal lamina and glia limitans.^{27,28,39} As recently reviewed in this journal,²³ both *GLIALCAM* and *MLC1* mutations cause MLC^{24,27}, a disease characterized by myelin vacuolation in the cerebral white matter, relatively sparing the corpus callosum, internal capsule, brainstem and cerebellum.^{21,22} MLC1 is involved in chloride currents necessary for the astrocytic regulatory volume decrease following cell swelling.⁴⁰ GlialCAM is a cell adhesion molecule indispensable for correct localization of MLC1 and CIC-2.^{27,28} Our study indicates that CIC-2 is part of the same ion and water homeostatic pathways as MLC1 and GlialCAM (Figure S9).

A limitation of the present study is the rather small number of patients. The database on unclassified leukoencephalopathies in Amsterdam contains over 3000 patients and only few patients fulfilled the MRI criteria. We analyzed several more adult and pediatric patients who did not fully fulfill the MRI inclusion criteria and did not find *CLCN2* mutations in any of those. It could be that the CIC-2 related leukoencephalopathy is very rare, but we cannot exclude the possibility that the phenotypic variation is much wider and that we have not analyzed a sufficient number of patients yet.

Many questions remain. The exact role of CIC-2 in brain ion and water homeostasis is unknown. It is unclear why defects in the same pathways cause different white matter

disorders. CIC-2- and Cx32-related disease preferentially affects white matter structures relatively spared by MLC1- and GlialCAM-related disease. While recessive mutations in *MLC1* and *GLIALCAM* lead to diffuse cerebral white matter edema, relatively sparing the corpus callosum, internal capsule, brain stem and cerebellum, recessive mutations in *CLCN2* and *GJB1* preferentially cause white matter edema of the internal capsule, brain stem structures and cerebellum. Another intriguing question concerns the size of the myelin vacuoles. In MLC, ADC values in the affected white matter are highly increased,⁴¹ indicating large vacuoles and increased extracellular spaces, as confirmed by EM.²² In CIC-2- and Cx32-related disease, ADC values in affected white matter are low, indicating small intramyelinic vacuoles and extracellular spaces. Although GlialCAM is supposed to be a chaperone for both MLC1 and CIC-2, recessive *GLIALCAM* mutations lead to a disease that is indistinguishable from the disease caused by *MLC1* mutations and does not share the MRI features of the disease caused by *CLCN2* mutations. Strikingly, we found that GlialCAM and MLC1 share restricted localization in distal astrocytic processes, whereas CIC-2 has a more diffuse membrane localization in astrocytes. These disease observations suggest that GlialCAM is a straightforward chaperone for MLC1, but that its relationship with CIC-2 is more complex.

The growing group of known disorders affecting brain ion and water homeostasis are typically relatively mild and slow, both in mice^{5,6,20,36} and humans.^{21,25,27,37} Probably the process of volume regulation in the brain is so important, that it relies on many different proteins and processes. Mutations in a single protein only lead to partial and sometimes transient dysfunction. It is important to note that intramyelinic edema can be reversible. Patients with MLC, caused by dominant *GLIALCAM* mutations, improve or recover.^{25,27} In most patients with a *GJB1* mutation, the white matter disease is transient.³⁷ If means are found to target components of the ion and water homeostatic pathways, myelin edema may be successfully combated.

Panel: Research in context

We did not do a systematic review. This work stems from discoveries made in our laboratories. We defined a novel leukoencephalopathy by the following MRI criteria: signal abnormalities in the posterior limbs of the internal capsules, midbrain cerebral peduncles and middle cerebellar peduncles. We found this pattern in three adult and four pediatric patients. Strikingly, diffusion restriction was found in those structures in all patients, suggesting myelin micro-vacuolation. The adult patients had additional variable, mild and nonspecific cerebral hemispheric white matter abnormalities. The pediatric patients had additional diffuse cerebral white matter abnormalities with restricted diffusion. Through exome sequencing followed by Sanger sequencing and mRNA analysis of the candidate genes we discovered mutations in *CLCN2*, encoding the chloride channel CIC-2, in three adult and three pediatric patients, and a mutation in *GJB1*, encoding connexin32, in one pediatric patient. Functional analysis showed that the *CLCN2* mutations cause loss of CIC-2 function. We demonstrated CIC-2 expression in all components of the pial syncytium: astrocytes, oligodendrocytes and ependymal cells. We showed that CIC-2 is enriched in perivascular endfeet, where GlialCAM and MLC1 are also expressed. GlialCAM and MLC1 immunoreactivity overlapped completely and extended further distally than CIC-2 into astrocytic endfeet. Connexin32 is known to be present in paranodal myelin and in contacts between myelin and astrocytes.

Interpretation

Brain white matter mainly consists of myelinated axons and its most important function is impulse conduction. Action potentials are based on shifts in ions, which are obligatorily associated with osmotically driven shifts in water, requiring rapid compensation. Any disturbance of the compensatory mechanisms may disrupt impulse transmission or lead to life threatening changes in brain volume. Astrocytes are central in the complex processes of brain ion and water homeostasis. They prevent action potential-induced intramyelinic edema by a process called “potassium siphoning”. Past studies have shown that connexin32, MLC1 and GlialCAM are molecular components of these water and ion homeostatic pathways.

CLCN2 mutations have been implicated in idiopathic epilepsies, but this suggestion has been the subject of heated debates for a decade and the original paper had to be withdrawn. The present study provides no evidence for a role of *CLCN2* mutations in epilepsy and should put a definitive end to the discussion. In contrast, it shows that CIC-2 is involved in brain ion and water homeostasis. Strikingly, defects in MLC1, GlialCAM, connexin32 and CIC-2 all lead to leukoencephalopathies characterized by intramyelinic edema. Observations in X-linked Charcot-Marie-Tooth disease caused by *GJB1* mutations, and MLC caused by dominant *GLIALCAM* mutations indicate that intramyelinic edema can be reversible. If means are found to target components of the ion and water homeostatic pathways, this edema may be successfully combated. The present paper demonstrates that CIC-2 is one of the molecular components and may be a potential therapeutic target.

Contributors

C.De., M.B., C. Du., N.P., C.v.B., E. P., T.E.M.A., have performed and/or analyzed the experiments. C.De., F.S. and M.v.d.K. have designed and supervised the study. C.De. and M.v.d.K. have written the first draft of the manuscript. D.G., V. T., E.T., F.D., A.B., C. E. d.D.-S., J.S.V., A.V., G.U., C.Y., S.G.F, V.M.K., J.K., M.K., and N.I.W. contributed to patient data and/or materials essential to the study. All coauthors have critically reviewed and approved the last version of the manuscript.

Conflict of interest

We declare that we have no conflict of interest

Acknowledgements

We thank patients and families for their participation to the study. We thank the following practitioners for their identification and referral of patients: Janell Kierstein, CGC, Johan van Hove, MD, and Abigail Collins, MD, the Children's Hospital of Denver, and Johanna L. Schmidt, CGC, Children's National Medical Center Washington. We thank Raúl Estévez, PhD, University of Barcelona, for the anti-MLC1 antibody, and the Dutch Brain Bank for providing part of the tissue used in the study. We thank James M. Powers, MD, University of Rochester, for critical reading of the manuscript. We thank the PIC-PS platform of CRICM and the genotyping and sequencing platform of ICM for technical assistance, the DNA and cell bank of CRICM for DNA extraction and cell culture, Kees van Rozendaal, Department of Clinical Genomics, Maastricht University Medical Center, for assistance in the exome sequencing of patient 7 and his family, and Petra J.W. Pouwels, MR physicist, VU University Medical Center, Amsterdam, for her help in analysis of the ADC maps.

References

1. Planells-Cases R, Jentsch TJ. Chloride channelopathies. *Biochim Biophys Acta*. **2009** Mar;1792(3):173-89.
2. Thiemann A, Grunder S, Pusch M, Jentsch TJ. A chloride channel widely expressed in epithelial and non-epithelial cells. *Nature*. **1992** Mar 5;356(6364):57-60.
3. Grunder S, Thiemann A, Pusch M, Jentsch TJ. Regions involved in the opening of CIC-2 chloride channel by voltage and cell volume. *Nature*. **1992** Dec 24-31;360(6406):759-62.
4. Jordt SE, Jentsch TJ. Molecular dissection of gating in the CIC-2 chloride channel. *EMBO J*. **1997** Apr 1;16(7):1582-92.
5. Bosl MR, Stein V, Hubner C, et al. Male germ cells and photoreceptors, both dependent on close cell-cell interactions, degenerate upon CIC-2 Cl(-) channel disruption. *EMBO J*. **2001** Mar 15;20(6):1289-99.
6. Blanz J, Schweizer M, Auberson M, et al. Leukoencephalopathy upon disruption of the chloride channel CIC-2. *J Neurosci*. **2007** Jun 13;27(24):6581-9.
7. Sik A, Smith RL, Freund TF. Distribution of chloride channel-2-immunoreactive neuronal and astrocytic processes in the hippocampus. *Neuroscience*. **2000**;101(1):51-65.
8. Smith RL, Clayton GH, Wilcox CL, Escudero KW, Staley KJ. Differential expression of an inwardly rectifying chloride conductance in rat brain neurons: a potential mechanism for cell-specific modulation of postsynaptic inhibition. *J Neurosci*. **1995** May;15(5 Pt 2):4057-67.
9. Rinke I, Artmann J, Stein V. CIC-2 voltage-gated channels constitute part of the background conductance and assist chloride extrusion. *J Neurosci*. **2010** Mar 31;30(13):4776-86.
10. Ratte S, Prescott SA. CIC-2 channels regulate neuronal excitability, not intracellular chloride levels. *J Neurosci*. **2011** Nov 2;31(44):15838-43.
11. Haug K, Warnstedt M, Alekov AK, et al. Mutations in CLCN2 encoding a voltage-gated chloride channel are associated with idiopathic generalized epilepsies. *Nat Genet*. **2003** Apr;33(4):527-32.
12. D'Agostino D, Bertelli M, Gallo S, et al. Mutations and polymorphisms of the CLCN2 gene in idiopathic epilepsy. *Neurology*. **2004** Oct 26;63(8):1500-2.
13. Stogmann E, Lichtner P, Baumgartner C, et al. Mutations in the CLCN2 gene are a rare cause of idiopathic generalized epilepsy syndromes. *Neurogenetics*. **2006** Nov;7(4):265-8.
14. Everett K, Chioza B, Aicardi J, et al. Linkage and mutational analysis of CLCN2 in childhood absence epilepsy. *Epilepsy Res*. **2007** Jul;75(2-3):145-53.
15. Saint-Martin C, Gauvain G, Teodorescu G, et al. Two novel CLCN2 mutations accelerating chloride channel deactivation are associated with idiopathic generalized epilepsy. *Hum Mutat*. **2009** Mar;30(3):397-405.
16. Combi R, Grioni D, Contri M, et al. Clinical and genetic familial study of a large cohort of Italian children with idiopathic epilepsy. *Brain Res Bull*. **2009** Apr 29;79(2):89-96.
17. Kleefuss-Lie A, Friedl W, Cichon S, et al. CLCN2 variants in idiopathic generalized epilepsy. *Nat Genet*. **2009** Sep;41(9):954-5.
18. Haug K, Warnstedt M, Alekov AK, et al. Retraction: Mutations in CLCN2 encoding a voltage-gated chloride channel are associated with idiopathic generalized epilepsies. *Nat Genet*. **2009** Sep;41(9):1043.
19. Niemeyer MI, Cid LP, Sepulveda FV, et al. No evidence for a role of CLCN2 variants in idiopathic generalized epilepsy. *Nat Genet*. **2010** Jan;42(1):3.
20. Edwards MM, Marin de Evsikova C, Collin GB, et al. Photoreceptor degeneration, azoospermia, leukoencephalopathy, and abnormal RPE cell function in mice expressing an early stop mutation in CLCN2. *Invest Ophthalmol Vis Sci*. **2010** Jun;51(6):3264-72.
21. van der Knaap MS, Barth PG, Stroink H, et al. Leukoencephalopathy with swelling and a discrepantly mild clinical course in eight children. *Ann Neurol*. **1995** Mar;37(3):324-34.
22. van der Knaap MS, Barth PG, Vrensens GF, Valk J. Histopathology of an infantile-onset spongiform leukoencephalopathy with a discrepantly mild clinical course. *Acta Neuropathol*. **1996** Aug;92(2):206-12.
23. van der Knaap MS, Boor I, Estevez R. Megalencephalic leukoencephalopathy with subcortical cysts: chronic white matter oedema due to a defect in brain ion and water homeostasis. *Lancet Neurol*. **2012** Nov;11(11):973-85.
24. Leegwater PA, Yuan BQ, van der Steen J, et al. Mutations of MLC1 (KIAA0027), encoding a putative membrane protein, cause megalencephalic leukoencephalopathy with subcortical cysts. *Am J Hum Genet*. **2001** Apr;68(4):831-8.
25. van der Knaap MS, Lai V, Kohler W, et al. Megalencephalic leukoencephalopathy with cysts without MLC1 defect. *Ann Neurol*. **2010** Jun;67(6):834-7.
26. Scheper GC, van Berkel CG, Leisle L, et al. Analysis of CLCN2 as candidate gene for megalencephalic leukoencephalopathy with subcortical cysts. *Genet Test Mol Biomarkers*. **2010** Apr;14(2):255-7.

27. Lopez-Hernandez T, Ridder MC, Montolio M, et al. Mutant GlialCAM causes megalencephalic leukoencephalopathy with subcortical cysts, benign familial macrocephaly, and macrocephaly with retardation and autism. *Am J Hum Genet.* **2011** Apr 8;88(4):422-32.
28. Jeworutzki E, Lopez-Hernandez T, Capdevila-Nortes X, et al. GlialCAM, a protein defective in a leukodystrophy, serves as a CIC-2 Cl(-) channel auxiliary subunit. *Neuron.* **2012** Mar 8;73(5):951-61.
29. van der Knaap MS, Breiter SN, Naidu S, Hart AA, Valk J. Defining and categorizing leukoencephalopathies of unknown origin: MR imaging approach. *Radiology.* **1999** Oct;213(1):121-33.
30. Schiffmann R, van der Knaap MS. Invited article: an MRI-based approach to the diagnosis of white matter disorders. *Neurology.* **2009** Feb 24;72(8):750-9.
31. Dreha-Kulaczewski SF, Brockmann K, Henneke M, et al. Assessment of myelination in hypomyelinating disorders by quantitative MRI. *J Magn Reson Imaging.* **2012** Aug 21.
32. Patay Z. Diffusion-weighted MR imaging in leukodystrophies. *Eur Radiol.* **2005** Nov;15(11):2284-303.
33. Benfenati V, Ferroni S. Water transport between CNS compartments: functional and molecular interactions between aquaporins and ion channels. *Neuroscience.* **2010** Jul 28;168(4):926-40.
34. Rash JE. Molecular disruptions of the panglial syncytium block potassium siphoning and axonal saltatory conduction: pertinence to neuromyelitis optica and other demyelinating diseases of the central nervous system. *Neuroscience.* **2010** Jul 28;168(4):982-1008.
35. Neusch C, Rozengurt N, Jacobs RE, Lester HA, Kofuji P. Kir4.1 potassium channel subunit is crucial for oligodendrocyte development and in vivo myelination. *J Neurosci.* **2001** Aug 1;21(15):5429-38.
36. Menichella DM, Majdan M, Awatramani R, et al. Genetic and physiological evidence that oligodendrocyte gap junctions contribute to spatial buffering of potassium released during neuronal activity. *J Neurosci.* **2006** Oct 25;26(43):10984-91.
37. Paulson HL, Garbern JY, Hoban TF, et al. Transient central nervous system white matter abnormality in X-linked Charcot-Marie-Tooth disease. *Ann Neurol.* **2002** Oct;52(4):429-34.
38. Siskind C, Feely SM, Bernes S, Shy ME, Garbern JY. Persistent CNS dysfunction in a boy with CMT1X. *J Neurol Sci.* **2009** Apr 15;279(1-2):109-13.
39. Boor PK, de Groot K, Waisfisz Q, et al. MLC1: a novel protein in distal astroglial processes. *J Neuropathol Exp Neurol.* **2005** May;64(5):412-9.
40. Ridder MC, Boor I, Lodder JC, et al. Megalencephalic leukoencephalopathy with cysts: defect in chloride currents and cell volume regulation. *Brain.* **2011** Nov;134(Pt 11):3342-54.
41. van der Voorn JP, Pouwels PJ, Hart AA, et al. Childhood white matter disorders: quantitative MR imaging and spectroscopy. *Radiology.* **2006** Nov;241(2):510-7.

Table 1. *CLCN2* and *GJB1* mutations

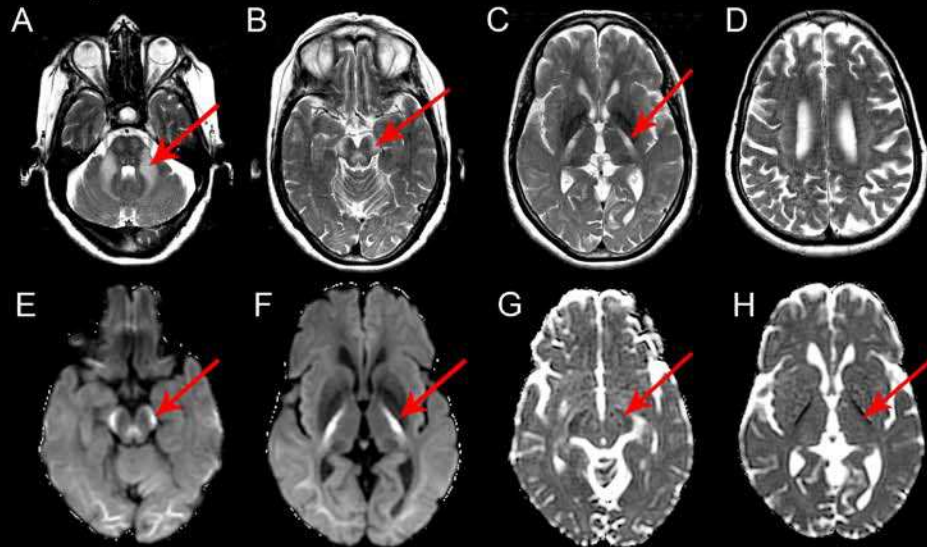
Patient	DNA	RNA	Exon	Protein	State	F/M
<i>CLCN2</i>						
1	c.1709G>A		15	p.Trp570*	Hom	n.a.
2	c.1709G>A		15	p.Trp570*	Hom	n.a.
3	c.430_435del		4	p.Leu144_Ile145del	Hom	n.a.
4	c.1143delT	r. 1143delT	11	p.Gly382Alafs*34	Het	n.a.
	c.64-1107_639del	r.64_639delins82 ^a	2-part 6	p.Met22Leufs*5	Het	n.a.
5	c.1499C>T	r.1499C>T	14	p.Ala500Val	Hom	F+M
6	c.828dupG	n.a.	8	p.Arg277Alafs*23	Hom	F+M
<i>GJB1</i>						
7	c.520C>T		2	p.Pro174Ser	Hemi	M

Hom, homozygous; Het, heterozygous; Hemi, hemizygous ; n.a., not available; F, father ; M, mother

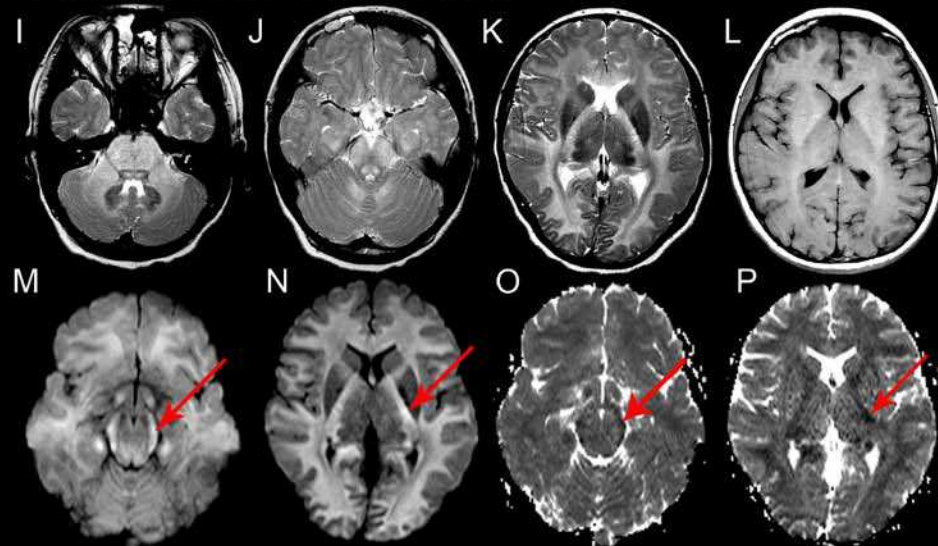
^a The *CLCN2* r.64_639delins82 variant comprises a deletion of exons 2-5 and part of exon 6 and the insertion of intron 1 c.63+1097_64-1108.

Figures

Adult patient with *CLCN2* mutations



Pediatric patient with *CLCN2* mutations



Patient with *GJB1* mutation

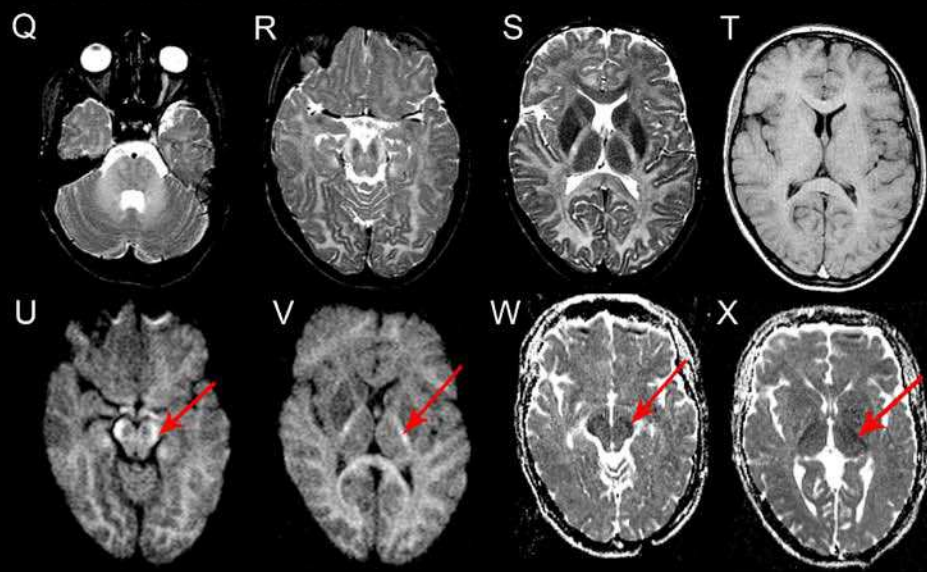


Figure 1. Magnetic resonance imaging

MRI in patient 1 at the age of 63 years (A-H) shows signal abnormalities on T₂-weighted images (A-D) in the middle cerebellar peduncles (arrow in A), midbrain cerebral peduncles (arrow in B) and posterior limbs of the internal capsules (arrow in C). Slight signal abnormalities are present in the cerebral white matter (D). Diffusion-weighted images (E, F) demonstrate high signal in the midbrain cerebral peduncles (arrow in E), posterior limbs of the internal capsules (arrow in F) and to a lesser degree the posterior subcortical cerebral white matter (compare hyperintense posterior white matter to normal anterior white matter in E and F), suggesting restricted diffusion, confirmed by low ADC values on the ADC maps (low signal in G and H, arrows). *MRI in patient 4 at the age of 14 years (I-P)* shows diffuse mild T₂-hyperintensity (I-K) and T₁-hyperintensity (L) of all white matter structures. Prominent T₂-hyperintensity is seen in the basis pontis (I), middle cerebellar peduncles (I), midbrain cerebral peduncles (J), and posterior limbs of the internal capsules (K). Diffusion-weighted images (M, N) show increased signal in virtually all white matter, especially the midbrain cerebral peduncles (arrow in M) and posterior limbs of the internal capsules (arrow in N), suggesting restricted diffusion, confirmed by low ADC values on the ADC maps (arrows in O and P). *MRI in patient 7 at the age of 14 years (Q-X)* shows diffuse mild T₂-hyperintensity (Q-S) and T₁-hyperintensity (T) of all white matter structures. Prominent T₂-hyperintensity is seen in the middle cerebellar peduncles (Q), midbrain cerebral peduncles (R), and posterior limbs of the internal capsules (S). Diffusion-weighted images (U, V) show mildly increased signal in almost all white matter, especially the midbrain cerebral peduncles (arrow in U) and posterior limbs of the internal capsules (arrow in V), suggesting restricted diffusion, confirmed by low ADC values on the ADC maps (arrows in W and X).

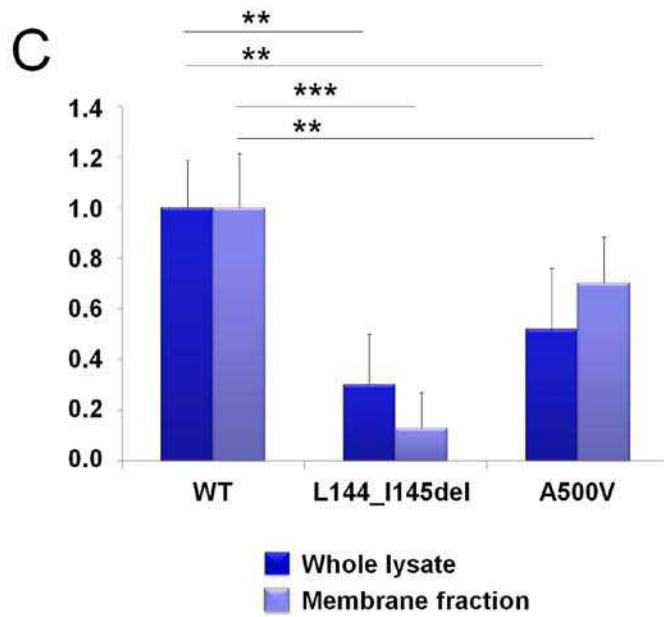
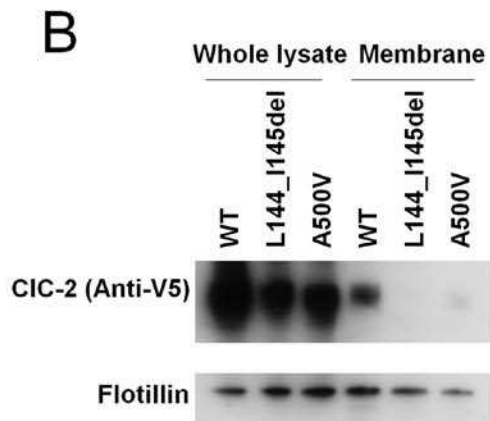
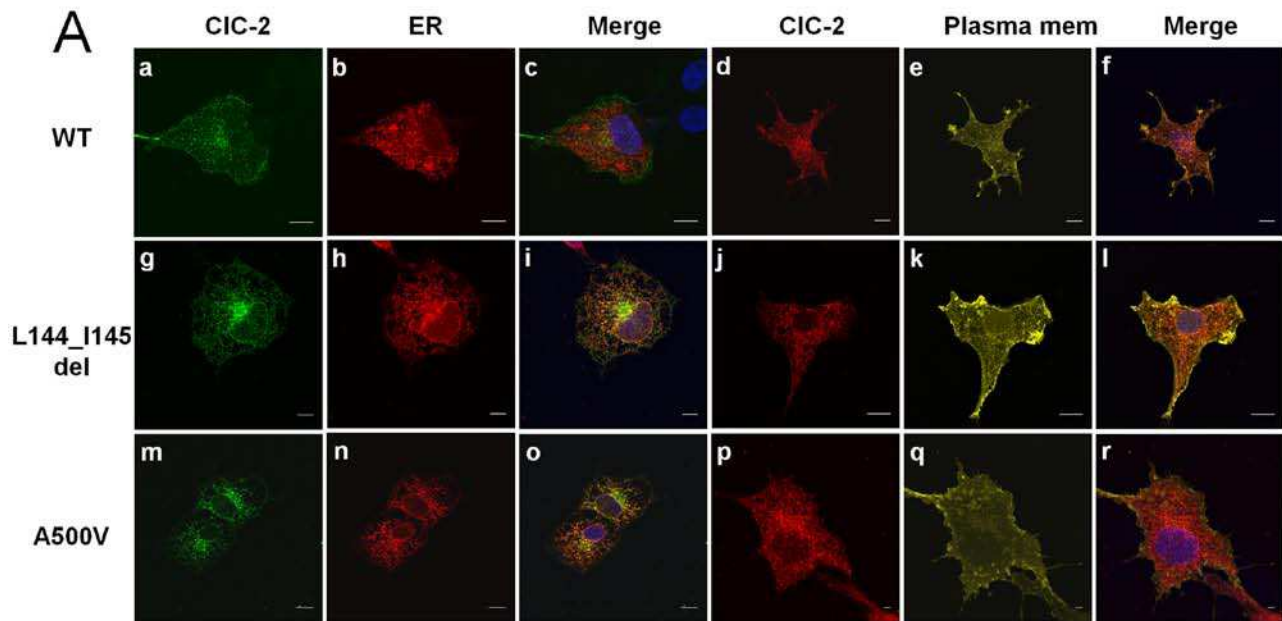


Figure 2. Functional consequences of *CLCN2* mutations

A) Subcellular localization of wild-type (WT) (a-f) and mutated (p.Leu144_Ile145del: g-l; p.Ala500Val: m-r) CIC-2 proteins and colocalization with markers of endoplasmic reticulum (anti-calreticulin, red, b, h, n) or plasma membrane (pEYFP-Mem, yellow, e, k, q) by confocal microscopy. Note that WT CIC-2 is present at the plasma membrane and different subcellular compartments, whereas both mutant proteins are mainly observed in the endoplasmic reticulum. Scale bar: 10 μ m. B) Quantification of co-localization of wild-type or mutated (p.Leu144_Ile145del, p.Ala500Val) proteins with endoplasmic reticulum and plasma membrane using the Pearson correlation coefficient, including at least 3 cells per group. * $P < 0.05$. C) Analysis of WT and mutated CIC-2 protein expression in whole lysates and plasma membranes by Western blot show that the amount of mutant CIC-2 protein transiently expressed in Cos7 cells is decreased compared to the WT form, especially in the plasma membrane. The image shows the result of a representative experiment. Flotillin was used to control and normalize the protein load. D) Quantification of WT and mutant CIC-2 proteins present in whole lysates and in plasma membranes shows that mutant CIC-2 proteins are globally less expressed than WT CIC-2, suggesting that they are misfolded and instable. Contrary to the WT form, both mutants are retained in the endoplasmic reticulum, where they are likely degraded and hardly reach the plasma membrane. The values, obtained from at least three different experiments, were compared with the Mann-Whitney test; **: $p < 0.01$; ***: $p < 0.001$.

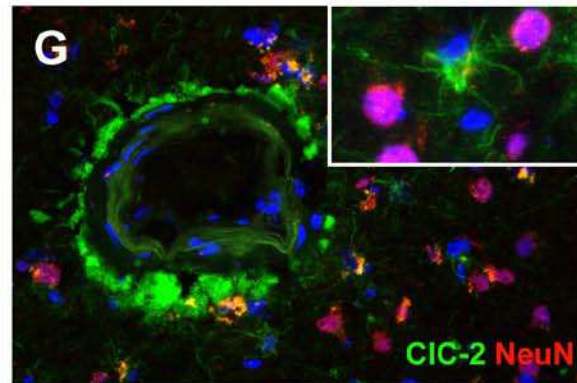
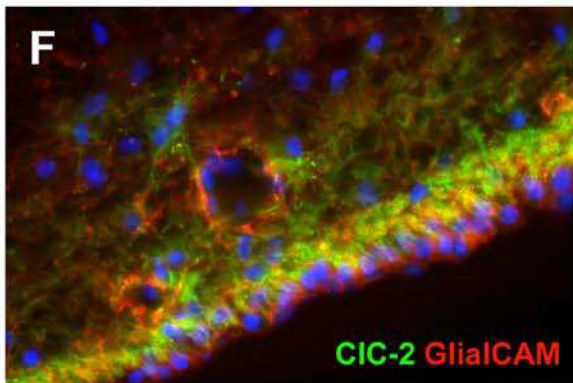
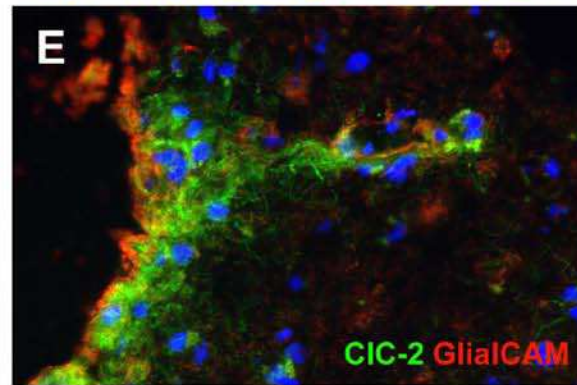
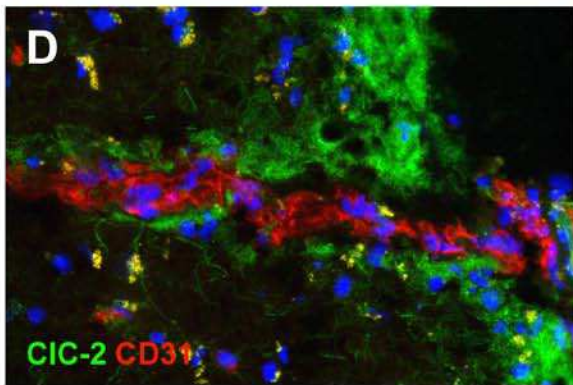
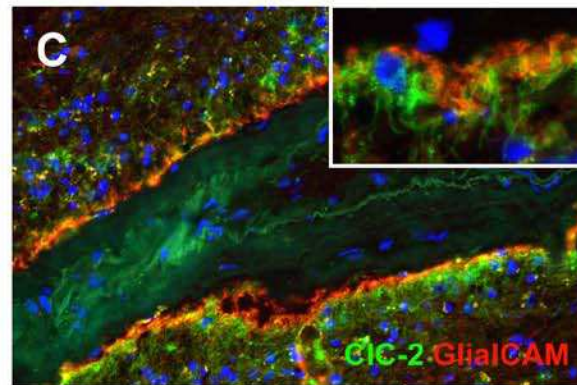
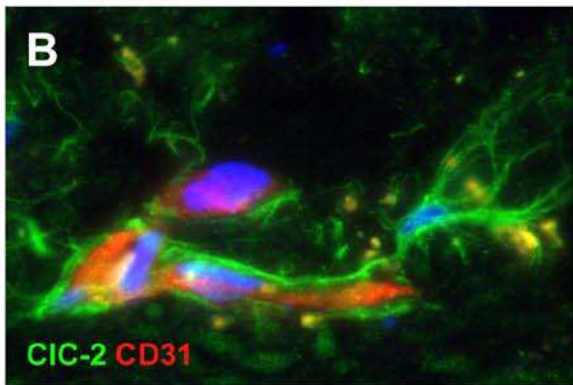
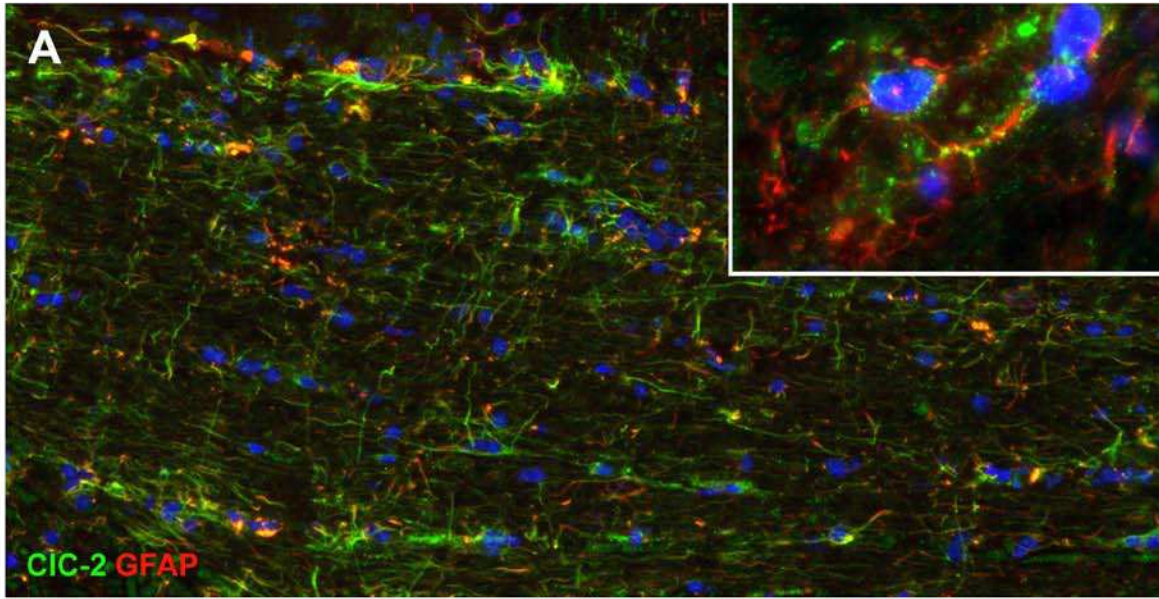


Figure 3. Immunohistochemistry: expression of CIC-2 in the normal adult human brain. Double staining of the cerebral white matter for CIC-2 (green) and the astrocyte-specific marker GFAP (red) shows that all GFAP⁺ astrocytes express CIC-2 (A). Note the long CIC-2⁺ astrocytic processes extending parallel and perpendicular to the direction of the fiber bundle. CIC-2 shows a punctate immunoreactivity, as expected for a membrane protein (inset in A). Co-labeling of the same tissue for CIC-2 (green) and the vascular endothelial cell marker CD31 (red) shows that expression of CIC-2 is enhanced in the astrocytes surrounding the blood vessels deep in the parenchyma (B) as well as the penetrating vessels at the surface of the brain (D). Note the numerous fine astrocytic processes running along the white matter capillary (B). Perivascular astrocytes (C), subpial astrocytes (E) and ependymal cells (F) co-express GlialCAM (red) with CIC-2 (green), but GlialCAM immunoreactivity extends farther into the astrocytic processes and endfeet (inset in C). Double staining of the frontal cortex for CIC-2 (green) and the neuronal marker NeuN (red) shows that, in this location, CIC-2 immunoreactivity is limited to perivascular astrocytes (G). No CIC-2 expression is seen in the NeuN⁺ neuronal cells (inset in G). In all images the cell nuclei are stained with DAPI (blue). Original magnifications: (A) 100x, (B) 630x, (C, D, E, F and G) 200x, (insets) 400x.

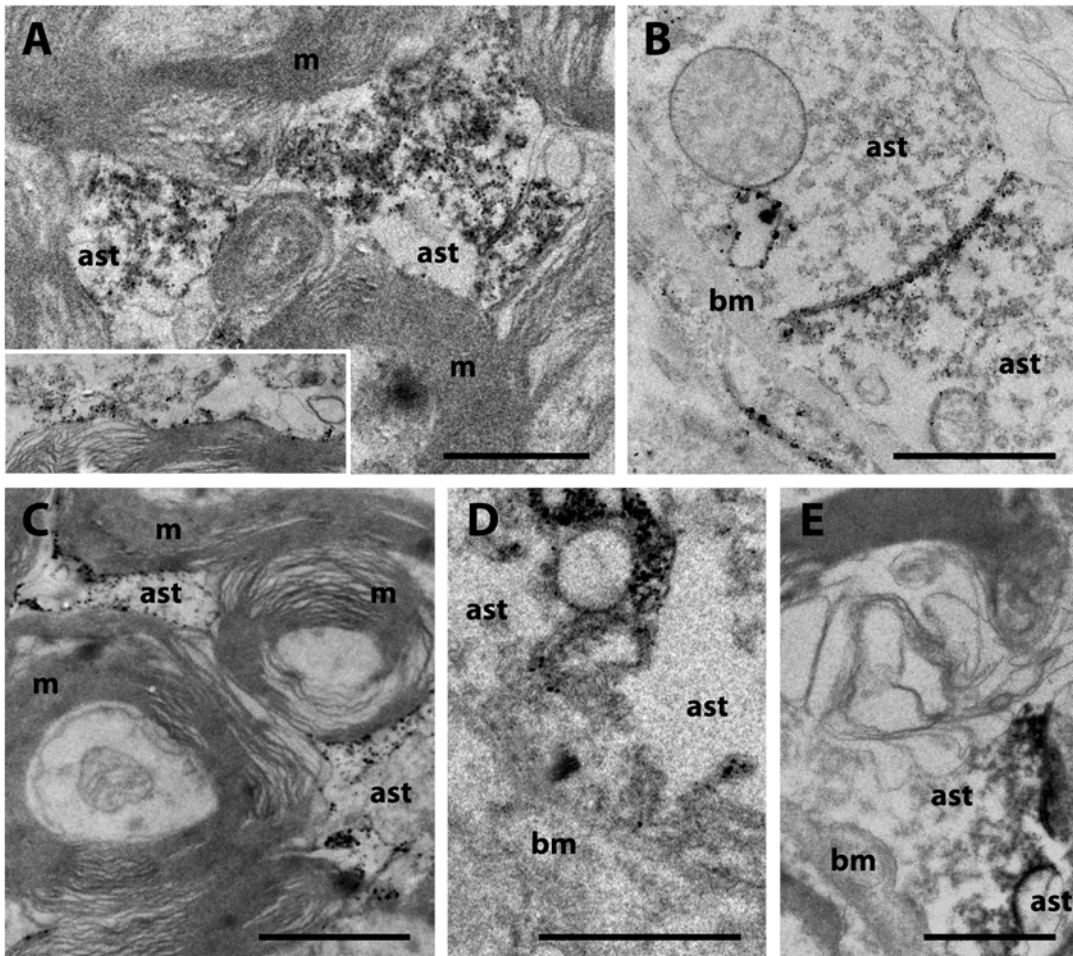


Figure 4. Electron microscopy: CIC-2, GlialCAM and MLC1 immunoreactivity in the normal adult white matter. CIC-2 is expressed on astrocytic processes in between myelinated axons (A) and in contact with abaxonal myelin (inset in A). A similar localization is observed for GlialCAM (C). Intense CIC-2 immunoreactivity is present in astrocytic endfeet surrounding blood vessels (B). Note the enhanced CIC-2 expression in the astrocyte-astrocyte contacts of the endfeet (B). At this site, GlialCAM (D) and MLC1 (E) are also expressed. Scale bars: 1 μ m; m, myelin; ast, astrocyte; bm, basement membrane.

Supplementary methods

Exome sequencing and Sanger sequencing

The exonic regions of the genome of the three patients with adult-onset disease were sequenced by DNAvision (Charleroi, Belgium). Genomic DNA was captured using the SureSelect Human All Exon 50 Mb kit (Agilent), followed by 75 base pair paired-end massively parallel sequencing on a HiSeq2000 sequencing system (Illumina), according to the manufacturers' instruction and protocols. Reads were mapped onto the reference genome (hg19) using the Burrows-Wheeler Aligner software.^{1,2} Removing of duplicated reads and mutation calling were performed using samtools^{1,2} according to the following criteria: position coverage greater or equal to 20, mutation proportion greater or equal to 25%, and mutated bases called at least 10% on each strand.

The analysis of exome data assumed an autosomal recessive inheritance and was first based on the search for homozygous mutations located in identical-by-descent regions in patient 3. Possibly deleterious variants (i.e. with possible impact on gene or protein function) were defined as indels introducing frameshifts or in-frame insertions / deletions, nonsense or splice site mutations, mutations altering start or termination codons, or missense variants predicted at least once *in silico* to be deleterious and absent or not validated in control databases. Genes with at least one homozygous variant or at least two least two heterozygous variants predicted deleterious were listed for the three adult patients. The final analysis excluded possibly deleterious variants also detected

in 7 exomes of individuals with other diseases performed at the same time to exclude false-positives and frequent variants not reported in databases.

The exons and intron-exon junctions of *CLCN2* (accession number NG_016422.1) were amplified and analyzed in these three adult patients, as described.³ In the four selected patients with pediatric-onset disease, the exons and intron-exon junctions of *CLCN2* were also sequenced, as described.⁴ Primer sets were designed to amplify exons for the longest transcript variant (accession number NM_004366.4) with Primer3 (<http://frodo.wi.mit.edu/primer3/>). They are listed in Table S8. In those pediatric patients in whom no mutations were found or only one, *CLCN2* mRNA was isolated from lymphoblasts and reverse-transcribed. *CLCN2* cDNA was amplified in four overlapping fragments, which were sequenced using primers listed in Table S6.

In the fourth patient, who had the X-linked disease the exons and intron-exon junctions of *GJB1* (accession number NG_008357.1) were amplified and analyzed (primers listed in Table S8).

Mutation interpretation was assessed using Alamut2.1 (Interactive Biosoftware), shown in Table S7. The *CLCN2* and *GJB1* mutation nomenclature is based on the cDNA reference sequences (NM_004366.4 and NM_000166.5 respectively), according to HGVS recommendations (www.hgvs.org/mutnomen).

Functional studies

CLCN2 mRNA was quantified in available fibroblasts of two adult patients with *CLCN2* mutations. Half of the cells were pretreated overnight with 10 µg/ml

emetin to inhibit nonsense-mediated decay (NMD). Total RNA was isolated using the Qiagen RNeasy Mini kit (Invitrogen). First-strand synthesis was performed with 1 µg of total RNA using the SuperScript III First-Strand Kit (Invitrogen). Quantification was carried out using the Qiagen QuantiTect primer assays for *CLCN2*, *PPIA* and *GAPDH* were used as control genes. Each sample was run in triplicate on a Lightcycler-480 apparatus (Roche). Forty-five two-step cycles (30 s at 95°C and 30 s at 60°C) were performed. Analysis was performed using qbase Plus software (Biogazelle).

Cos7 cells were transiently co-transfected with 5 µg of CIC-2-V5-His6 expression plasmids³ and pEYFP-Mem (Plasma membrane marker, Clontech) with a ratio 1:5, using a neon electroporation system (Invitrogen). For immunofluorescence staining, cells were fixed with 4% paraformaldehyde (PFA) 24h after transfection, permeabilized with 0.1% Triton X-100, and incubated with the primary antibody: monoclonal mouse anti-v5 (Abcam, ab27671, 1:10000), rabbit anti-CIC-2 (Sigma HPA024108, 1:200 or Santa Cruz SC-20122, 1:200), and/or anti-calreticulin (ER marker, Abcam, ab2907, 1:1000) for at least for 2 hours at room temperature. The signal was revealed by incubation with Alexa Fluor 488-coupled goat anti-rabbit or donkey anti-mouse IgG antibody (Invitrogen, 1:1000) or Cy3-coupled sheep anti-mouse or anti-rabbit IgG antibody (Sigma, 1:1000) for one hour at room temperature. Nuclei were stained with Hoescht (1:1000). Fluorescent images were acquired with a confocal system (Leica SP2 AOBS AOTF).

Proteins present at the plasma membrane were isolated following surface biotinylation on living Cos7 cells with the Cell Surface Protein Isolation Kit (Pierce), following the manufacturer's recommendations. Proteins were resolved by SDS-PAGE on 4–12% gradient gels (Invitrogen) and electrotransferred onto nitrocellulose membranes. CIC-2 was probed with anti-v5 or anti-CIC-2 antibodies and the signal was revealed by enhanced chemiluminescence (Pierce). The membranes were then probed with anti-Flotillin-1 (BD Biosciences 610820) antibody for normalization. The ImageJ program (<http://rsb.info.nih.gov/ij/>) was used for signal quantification and calculation of Pearson Coefficients. For mRNA quantification and biotinylation assay, independent measures from at least three different experiments were compared with the Mann-Whitney test.

Western blot analyses of endogenous CIC-2 in human brain tissue

To study CIC-2 expression, three CIC-2 antibodies were used: GTX113403 (GeneTex), SC-20122 (Santa Cruz), and HPA24108 (Sigma). The GTX113403 and SC-20122 antibodies were both raised against the N-terminal part of CIC-2, whereas the HPA24108 antibody was raised against the C-terminal domain. To validate whether these anti-CIC-2 antibodies specifically detect CIC-2 in human brain samples, we performed several control experiments. First, HEK293 cells were transfected with the CIC-2-V5-His6 expression plasmid³ using PEI.⁵ Mock transfections were performed in parallel with pBlueScript. Lysates were prepared two days post-transfection as described.⁵ Equal amounts of protein were applied

to 11% SDS-PAGE without prior boiling, because boiling severely diminished CIC-2 detection with all tested antibodies (data not shown). The samples were subsequently transferred to Immobilon-P membrane (Millipore) overnight. Total protein loading was measured in-gel and on-blot with 2,2,2-trichloroethanol (TCE) that labels all tryptophans in the proteins.⁶ TCE imaging was performed with Bio-Rad Image Lab software.

Membranes were blocked in 5% non-fat milk in PBS- 0.1% Tween and incubated overnight at 4°C with primary antibody (1:1000 for GTX113403; 1:500 for SC-20122, 1:1000 for HPA24108 and 1:10000 for anti-v5). Subsequently, membranes were incubated with an HRP-conjugated secondary antibody (1:5000, Westburg) and further developed using the SuperSignal West Femto chemiluminescence-based detection kit (Pierce). Images were obtained with a Li-Cor Odyssey imager (Westburg) using the Image Studio software package.

We performed Western blot analyses with the same set of anti-CIC-2 antibodies on brain lysates prepared from two of the control individuals also investigated in fluorescent immunohistochemistry. Equal amounts of protein (~100 ug per well, as determined by Bradford analysis) were applied to 4%-12% gradient gels without prior boiling (NuPAGE system, Invitrogen). After transfer, membranes were handled as described above. To increase the sensitivity of the assay, the blots were incubated with a goat anti-rabbit IgG secondary antibody (1 hr, 4°C) and subsequently with an HRP-conjugated anti-goat IgG antibody (1 hr, 4°C).

We also performed immunocytochemistry on the transfected HEK293 cells with the GTX113403 anti-CIC-2 antibody (1:200). The signal was detected with the AF488-conjugated anti-rabbit IgG antibody (Molecular Probes, 1:400).

Immunohistochemistry and electron microscopy

To study the expression of CIC-2, MLC1 and GlialCAM, tissue samples from the posterior limb of the internal capsule, frontal white matter, frontal cortex and ependymal lining were obtained at autopsy from 9 unrelated control subjects aged 1 to 75 years (7 males, 2 females), who succumbed to heart disease (lymphocytic myocarditis or acute myocardial infarction) or extra-cerebral tumor (gastric or bladder carcinoma). None of the subjects had neurological symptoms. Routine neuropathologic examination, including gross examination of the brain on cut and review of Hematoxylin and Eosin-stained tissue sections from multiple brain areas, was normal in all cases.

For light-microscopy purposes, 8- μ m-thick frozen tissue sections were mounted on glass slides and fixed in 2% PFA, subsequently permeabilized with 0.1% saponin, blocked in 5% normal donkey serum and incubated with primary antibodies for 24 hours at 4°C. Immunohistochemistry was performed using antibodies against the following epitopes: glial fibrillary acidic protein (GFAP, Millipore, 1:1000); CIC-2 (GTX113403, 1:200; SC-20122, 1:20; HPA24108, 1:20); GlialCAM (R&D, 1:100); MLC1 (kind gift of Dr. R. Estévez, University of Barcelona, Spain, 1:100); oligodendrocyte transcription factor-2 (olig2, Millipore, 1:400); platelet endothelial cell adhesion molecule-1 (PECAM1/CD31, Dako,

1:50); neuronal nuclei (NeuN, Sigma, 1:500); phosphorylated neurofilaments (SMI31, Developmental Studies Hybridoma Bank, 1:1000); and non-phosphorylated neurofilament H (SMI32, Developmental Studies Hybridoma Bank, 1:1000). SMI31 and SMI32 antibodies were always applied simultaneously. In each experiment negative controls were included by omitting the primary antibody to verify the specificity of the immunohistochemical labeling. Specifically for the GTX113403 antibody, we included an isotype control rabbit IgG (SC-2027, Santa Cruz, 1:200). Furthermore, we performed a blocking experiment with this antibody. In brief, the protein (aa 27-303 of CIC-2; GTX113403-PEP_SAMP, GeneTex) used to raise the GTX113403 antibody was pre-incubated with GTX113403 in a 100-fold molar excess for 2 hours at 4°C whilst rotating. A control reaction was included in which the antigen was omitted.

After staining with secondary antibodies (Alexa 488-, 568-, and 594-tagged, Molecular Probes, 1:400), sections were counterstained with DAPI (Molecular Probes, 10 ng/ml) and photographed using a Leica DM6000B microscope (Leica Microsystems BV, Rijswijk, The Netherlands).

For electron microscopy (EM) purposes, tissue sections were fixed in 4% PFA, cryoprotected in 12.5% and 25% sucrose and frozen. Thirty to forty- μ m-thick frozen sections were incubated for 96 hours with antibodies against CIC-2, GlialCAM, or MLC1, and then rinsed before being incubated in a PowerVisionPoly-HRP-Goat Anti-rabbit IgG or Anti-mouse IgG (ImmunoVision Technologies Co., Daly City, CA). To visualize the peroxidase, sections were incubated in a Tris-HCl diaminobenzidine (DAB) solution containing 0.03% H₂O₂.

The DAB reaction product was then intensified by a gold-substituted silver peroxidase method.⁷ Sections were post-fixed for 20 minutes in 1% OsO₄ supplemented with 1% in potassium ferricyanide in sodium cacodylate buffer 0.1 M (pH 7.4). The material was then dehydrated and embedded in epoxy resin. Ultrathin sections, longitudinal to the cortico-spinal tract, were examined and photographed with a FEI Technai 12 electron microscope.

All pictures were acquired as TIFF files. The images were optimized for brightness and contrast using Photoshop, version 7.0 (Adobe systems, San Jose, CA).

Supplementary Tables

Table S1. MRI findings

Patient	1	2	3	4	5	6	7
Age at MRI	63	59	47	14	11	10	15
MRI consistent with hypomyelination	-	-	-	+	+	+	+
Posterior fossa abnormalities							
medulla							
central tegmental tracts	-	-	-	+	+	+	-
pons							
pyramidal tracts	+	+	+	+	+	+	+
medial lemniscus	+	-	-	-	-	-	-
central tegmental tracts	+	+	-	+	+	+	-
midbrain							
cerebral peduncles	+	+	+	+	+	+	+
central tegmental tracts	+	+	+	+	+	+	-
decussation sup.cerebel.ped.	+	+	+	-	-	-	-
cerebellar peduncles							
superior	+	+	+	-	-	-	-
middle	+	+	+	+	+	+	+
inferior	-	-	-	-	-	-	-
cerebellar white matter	+	+	+	+	+, partial	+	+
Cerebral abnormalities							
posterior limb internal capsule	+	+	+	+	+	+	+
anterior limb internal capsule	slight	-	-	(-)**	(-)**	(-)**	(-)**
corpus callosum	slight	slight	slight	(-)**	-	(-)**	(-)**
hemispheric white matter	diffuse, slight	diffuse, slight	multifocal	(-)**	(-)**	(-)**	(-)**
Diffusion restriction*							
posterior limb internal capsule	+	+	+	+	***	+	+
cerebral peduncles	+	+	-	+	***	+	+
middle cerebellar peduncles	+	-	-	+	-	+	+
elsewhere	borderline-low in part of cerebral subcortical white matter	-	-	borderline-low in most cerebral and cerebellar hemispheric white matter and corpus callosum	borderline-low in part of cerebral white matter***	borderline-low in most cerebral hemispheric white matter and corpus callosum	borderline-low in most cerebral and cerebellar hemispheric white matter and corpus callosum

* low ADC $\leq 60 \cdot 10^{-5} \text{mm}^2/\text{s}$; borderline-low ADC between 50 and $60 \cdot 10^{-5} \text{mm}^2/\text{s}$

** (-), signal consistent with lesion or hypomyelination

***, printed films available only, showing diffusion restriction, but no quantitative measurements possible

Table S2. Coverage of targeted exon sequences for adult patients

	Patient 1	Patient 2	Patient 3*
Reads on target	60.13%	60.84%	60.41%
Reads on target \pm 200	71.64%	72.57%	71.89%
Exon base coverage > 1	96.48%	96.99%	97.06%
Exon base coverage > 5	88.83%	89.79%	89.81%
Exon base coverage > 10	84.26%	85.39%	85.35%
Exon base coverage > 20	77.33%	78.29%	78.25%
Exon base coverage > 30	71.98%	72.44%	72.33%
Exon base coverage > 40	67.55%	67.46%	67.36%
Exon base coverage > 50	63.77%	63.20%	63.06%
Exon base coverage > 60	60.51%	59.46%	59.31%
Exon base coverage > 70	57.64%	56.12%	55.99%
Exon base coverage > 90	52.76%	50.26%	50.21%
Exon base coverage > 100	50.67%	47.64%	47.62%

*For patient 3 who has consanguineous parents, base coverage of homozygous regions exon was comprised between 75% and 93% with 84.4% of these regions being covered at least 20X.

Table S3. Statistics of the variants identified by exon sequencing in adult patients

	Total number of variants	SNPs	Indels	Variants in the homozygous state	Nonsense variants	Frameshifts	Missense variants
Patient 1	23117	21634	1483	8145	16	10	1190
Patient 2	24515	22937	1578	8880	10	14	1214
Patient 3	24234	22683	1551	9276	12	10	1327
Mean Number	23955	22418	1537	8767	13	11	1244

Table S4. Chromosomal coordinates (Hg18) of homozygous regions detected in patient 3 using Illumina cytoSNP-12 microarrays

Chr	Start	End	Size
1	77 177 872	85766226	8 588 355
1	111 542 465	121 013 322	9 470 858
1	148 082 160	161 140 149	13 057 990
1	161 141 595	164 091 790	2 950 196
2	45 711 744	47 108 563	1 396 820
3	180 007 441	195 701 202	15 693 762
5	149 045 840	167 700 692	18 654 853
6	106 405 154	139 889 414	33 484 261
8	43 243 823	66 327 538	23 083 716
13	27 572 026	29 648 616	2 076 591
13	70 205 497	75 619 664	5 414 168
13	75 629 803	94 661 781	19 031 979
13	94 701 436	98 091 589	3 390 154
15	25 852 901	42 883 194	17 030 294
15	68 121 272	76 023 408	7 902 137
15	76 102 552	87 366 490	11 263 939
17	73 051 214	74 822 865	1 771 652
19	8 979 319	15 713 242	6 733 924
19	15 714 080	24 423 444	8 709 365
19	32 615 675	36 073 126	3 457 452
20	10 077 600	13 027 630	2 950 031
20	34 031 506	40 113 764	6 082 259
Total			222 194 756

Table S5. List of SNPs and indels that are absent or rare in databases (MAF < 1%), have a possible impact and are located in regions homozygous by descent in patient 3

Chr.	Pos.	Ref. base	Mut. base	Type	Zygotity	Gene	Impact	AA change	Rs number
1	160062119	G	A	point	hom	<i>IGSF8</i>	missense	A560V	NA
3	184587274	A	G	point	hom	<i>VPS8</i>	missense	Y18C	rs61741194
3	1184076015	T	-GATGAG	del	hom	<i>CLCN2</i>	in-frame	144: LITFSA --> TFSA	NA
5	149907766	G	A	point	hom	<i>NDST1</i>	missense	R305H	NA
5	150563153	G	C	point	hom	<i>CCDC69</i>	missense	L246V	NA
6	128840288	T	G	point	hom	<i>PTPRK</i>	splice acceptor	NA	NA
13	29600208	G	A	point	hom	<i>MTUS2</i>	missense	R468Q	NA
15	42386638	C	A	point	hom	<i>PLA2G4D</i>	missense	G7V	NA
19	11305178	C	T	point	hom	<i>KANK2</i>	missense	V4I	NA
19	12258256	C	A	point	hom	<i>ZNF625</i>	missense	D49Y	NA
19	12258256	C	A	point	hom	<i>AC022415.5</i>	missense	D48Y	NA
20	11790885	C	+TT	ins	hom	<i>C20orf61</i>	frameshift	103: SM --> KV*	rs34383977

Table S6. Number of genes containing homozygous or compound heterozygous variants in the 3 adult patients

	<i>Number of autosomal genes with novel homozygous possibly deleterious variants</i>	<i>Number of autosomal genes with at least two novel heterozygous and possibly deleterious variants</i>	<i>Number of autosomal genes with novel homozygous or at least two heterozygous, possibly deleterious variants</i>
Patient 1	32	19	53
Patient 2	30	18	37
Patient 3	37	22	42
Number of genes common to ≥ 2 patients	14	8	24
Number of genes common to the 3 patients	5	5	11*
Number of genes common to the 3 patients considering only variants absent from exomes of patients with other diseases**			1 (CLCN2)

* List of the 11 genes containing homozygous or at least two heterozygous, possibly deleterious variants common to the 3 adult patients: **CLCN2**, *EXOC6B*, *KRTAP5-11*, *MPV17*, *MUC4*, *SEN3*, *SLC30A10*, *TAS2R43*, *TMPRSS13*, *ZNF717* and *ZNF880*.

** Most variants in the *EXOC6B*, *KRTAP5-11*, *MPV17*, *MUC4*, *SEN3*, *SLC30A10*, *TAS2R43*, *TMPRSS13*, *ZNF717* and *ZNF880* genes were identical in all three adult patients and were also present in exome data from individuals with other diseases analyzed at the same time (n=7). *MUC4* and *ZNF717* harbored multiple variants in all affected individuals and controls.

Table S7. Pathogenicity prediction for *CLCN2* and *GJB1* mutations

Mutation	effect	Conservation ^a		Align-GVGD ^b	Polyphen ^c	SIFT ^d	RNA ^e
		nucleotide	amino acid				
<i>CLCN2</i>^f							
c.64-1107_639del, p.Met22Leufs*5	out frame deletion, premature stop codon						NMD
c.430_435del ^g , p.Leu144_Ile145del	in frame deletion		up to <i>C. elegans</i>				
c.828dupG, p.Arg277Alafs*23	frameshift						NMD
c.1143delT, p.Gly382Alafs*34	frameshift						NMD
c.1499C>T, p.Ala500Val	missense	high (1.00)	up to <i>C. elegans</i>	C65	0.986	0.00	no effect
c.1709G>A, p.Trp570* ^g	premature stop codon						NMD
<i>GJB1</i>							
c.520C>T, p.Pro174Ser	missense	high (1.00)	up to fugu	C65	1.000	0.00	inconsistent

NMD, nonsense mediated decay

^a conservation was analyzed in 14 species for *CLCN2*, including human, chimp, orangutan, macaque, rat, mouse, dog, cat, cow, opossum, frog, tetraodon, fruitfly and *C. elegans*; in 15 species for *GJB1*, including human, chimp, macaque, rat, mouse, dog, cat, cow, armadillo, opossum, platypus, chicken, frog, tetraodon and fugu

^b C65 indicates most likely to interfere with function, C0 most unlikely

^c 0 (benign) - 1 (damaging)

^d [0.00-0.05] deleterious, [0.05-1.00] tolerated

^e RNA splicing prediction programs in the Alamut software include SpliceSiteFinder-like, MaxEntScan, NNSPLICE, Human Splicing Finder

^f *CLCN2* reference sequence NM_004366.4, *GJB1* NM_000166.5; none of the mutations is reported in the 1000 genomes and HapMap databases (www.1000genomes.org and www.hapmap.org).

^g not found in 180 locally available healthy controls, matched for ethnicity

Table S8. Oligonucleotides for *CLCN2* and *GJB1* sequencing

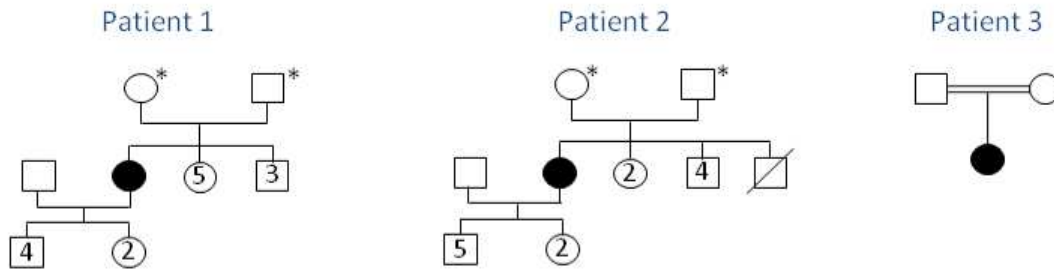
Primer name*	Sequence (5' → 3')
CLCN2-1Fa	CTCCACGTGCCAGTAGACC
CLCN2-1Ra	GGGAAGGACACCTGAGACAA
CLCN2-2+3F	CTGGGAGAAGAGGAGTGGAG
CLCN2-2+3R	AGAAGCCAAGACGCCTTCC
CLCN2-4F	ACAGCCTGTCGTATCAGCG
CLCN2-4R	AGCCTGGAGGGAACAGTC
CLCN2-5F	CCTCAGGCTGTCGGTATGTT
CLCN2-5R	AAGAGGGAGAGGAACTTGCTG
CLCN2-6F	ATGAAGGAGTCCCTCCTGGT
CLCN2-6R	CATTCTGGCGAGAGTGGTG
CLCN2-7F	AACCCTGGGGCAAGTAGG
CLCN2-7R	CTAAGGCCTCAGACCCAGAT
CLCN2-8+9+10F	CCTTGGCCTCTCCTCCTTG
CLCN2-8+9+10R	TTTACTGGGCCATTCTCTC
CLCN2-11+12F	GAGCCAAGGCTCTGCTCTG
CLCN2-11+12R	GAGAGGCTTCGAGGAGTGAG
CLCN2-13F	TAGACTTCTCCTGGGTGGC
CLCN2-13R	GGTGGGAAGAGAAAGAGGC
CLCN2-14F	GTGAGTTCTCAGCTGCCT
CLCN2-14R	GGACAGTCACACTCAGTCTC
CLCN2-15F	AGGGACCCACTCAGGACC
CLCN2-15R	GACCTTGCTAGAGGTGGCTG
CLCN2-16F	TGGAGCCCTCCTTGTGG
CLCN2-16R	CAAGGAGACTGGTCCTGAGC
CLCN2-17Fb	GCTCAGGACCAGTCTCCTTG
CLCN2-17Rb	CTTGAGTGCAGGCTTTAGGG
CLCN2-18+19F	GCAGGGTTATGACGTGGTC
CLCN2-18+19R	CTTCCAGGTGAGGGGAAAAG
CLCN2-20+21+22F	CACTGGCCTGAGTCCAAAC
CLCN2-20+21+22R	CTCCACCACTTCCCCTCAC
CLCN2-23Fb	CAGCAGTCCTGTCTCCTTCC
CLCN2-23Rb	ACCTCAGTGGTCTCCGTGTC
CLCN2-24Fb	AAGGAGGTGAGGTGATGGTG
CLCN2-24Rb	GCCTCTGGAAGACTTGTTGC
cCLCN2-1F	AGCCGAGTCCAGGACAGAG
cCLCN2-1R	AGAGGACGCCTCCAATAGGT
cCLCN2-2F	GCATCCCTGAGATGAAGACC
cCLCN2-2R	TAGGTGCTGCTGTCCGTATG
cCLCN2-3F	TGGTGGAGGAGCTAGAACCA
cCLCN2-3R	TGCTGGGAAGGCTGAGTC
cCLCN2-4F	ACAGGTGGTGGCATTGTTG
cCLCN2-4R	GCATGGCTAGCACCATCCTA
GJB1-1F	GAAAGACATGACCATCCTTCC
GJB1-1R	CGGATGATGAGGTACACCAC
GJB1-2F	GAAGAGGCACAAGGTCCA
GJB1-2R	GGAGGAAGGGAAGTAGCCA

* F forward, R reverse

Supplementary Figures

Figure S1. Pedigrees

A. Adult patients



* No known consanguinity but parents come from the same small village

B. CMTX family

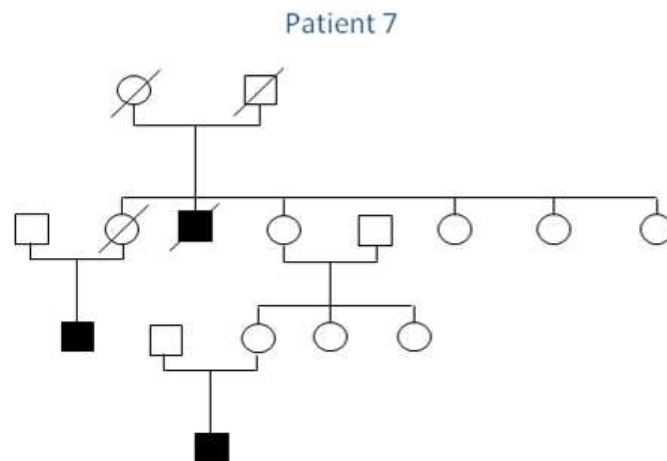
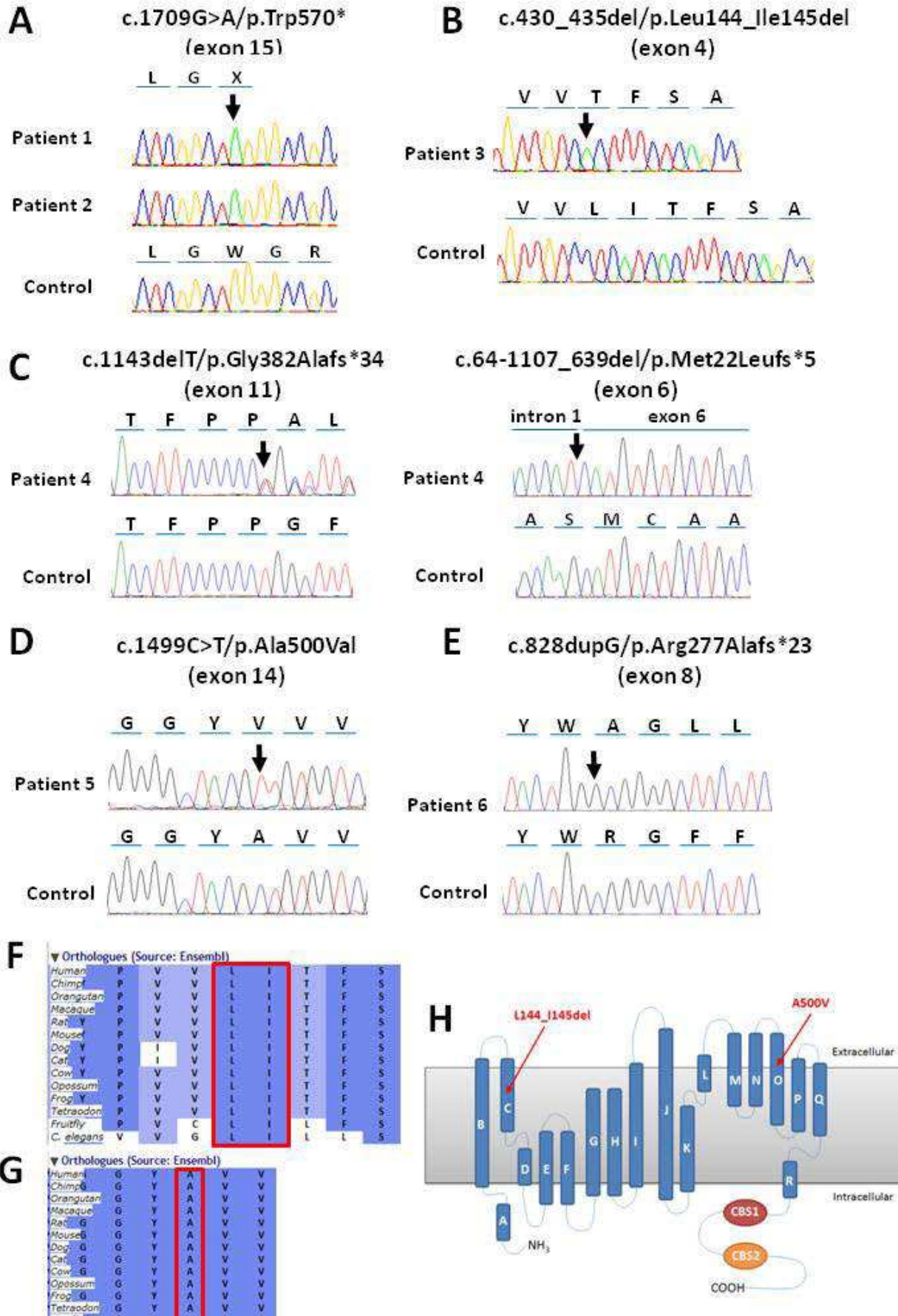
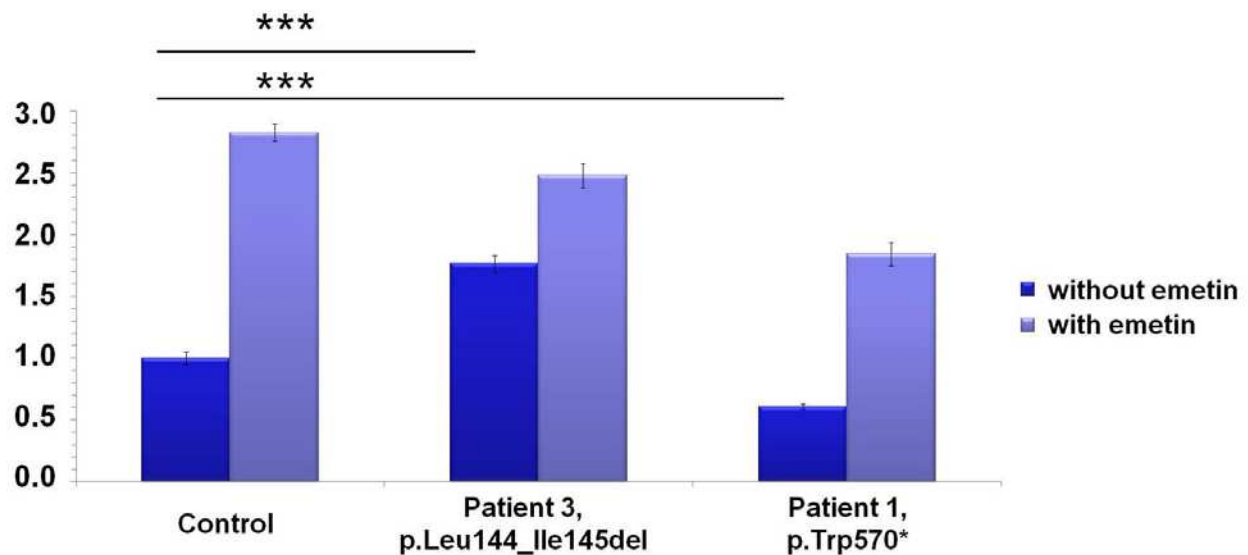


Figure S2. Confirmation of *CLCN2* mutations by Sanger sequencing and conservation of altered amino acids



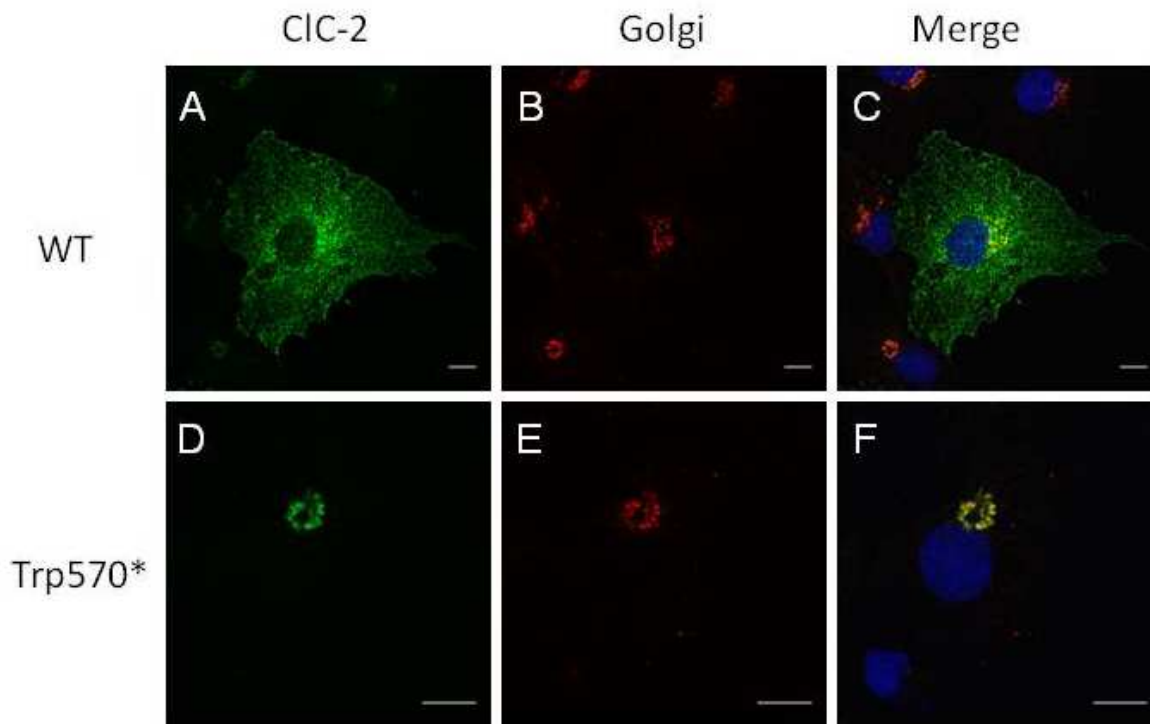
Sequence electropherograms of the c.1709G>A/p.Trp570* (A, patients 1 and 2), c430_435del/p.Leu144_Ile145del (B, patient 3), c.1143delT/p.Gly382AlafsX34 and c.64-1107_639del/p.Met22LeufsX5 (C, patient 4), c.1499C>T/p.Ala500Val (D, patient 5) and c.828dupG/p.Arg277AlafsX23 (E, patient 6) mutations in CLCN2. Mutation nomenclature is based on the CLCN2 transcript reference NM_004366. Nucleotides are numbered according to the cDNA with +1 corresponding to the A of the ATG translation initiation codon in the reference sequence. Orthologous protein alignments show that Leu144 and Ile145 (F) and Ala500 (G) are highly conserved during evolution (up to *C. elegans*). (H) Schematic representation of the CIC-2 channel showing the location of the p.Leu144_Ile145del and p.Ala500Val mutations in transmembrane domains of the CIC-2 protein. The topology of the CIC channel is based on a high resolution X-ray diffraction study of a CIC from *Salmonella typhimurium*.⁸

Fig. S3. Quantification of CLCN2 mRNA expression by real-time PCR



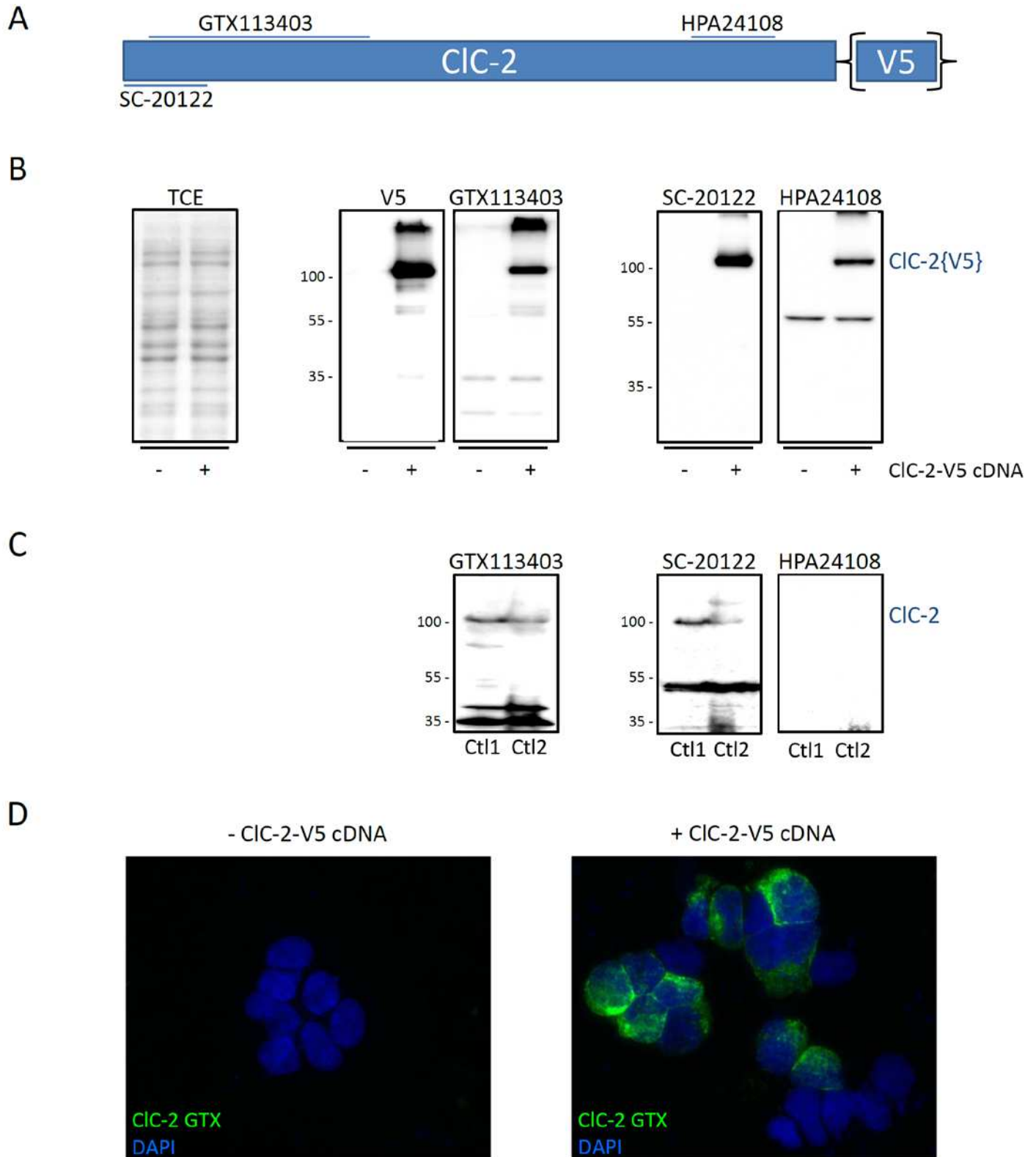
Quantification of CLCN2 expression in fibroblasts of patients 1 and 3 by real-time PCR showing that the Trp570* nonsense mutation specifically leads to CLCN2 mRNA down-regulation by nonsense-mediated decay (NMD), contrary to the Leu144_Ile 145 mutation. Treatment by emetin, a NMD-inhibitor, partially rescues mRNA expression although it also increases the mRNA levels in control individuals and in the patient with the Leu144_Ile 145 mutation. This result is compatible with the existence of many CLCN2 isoforms, some of which introducing premature termination codons.⁴ PPIA and GAPDH were used as control genes for normalization. Values were compared with the Mann-Whitney test; ***: $p < 0.001$.

Fig. S4. Aberrant cellular localization of the c.1709G>A, p.Trp570* mutation



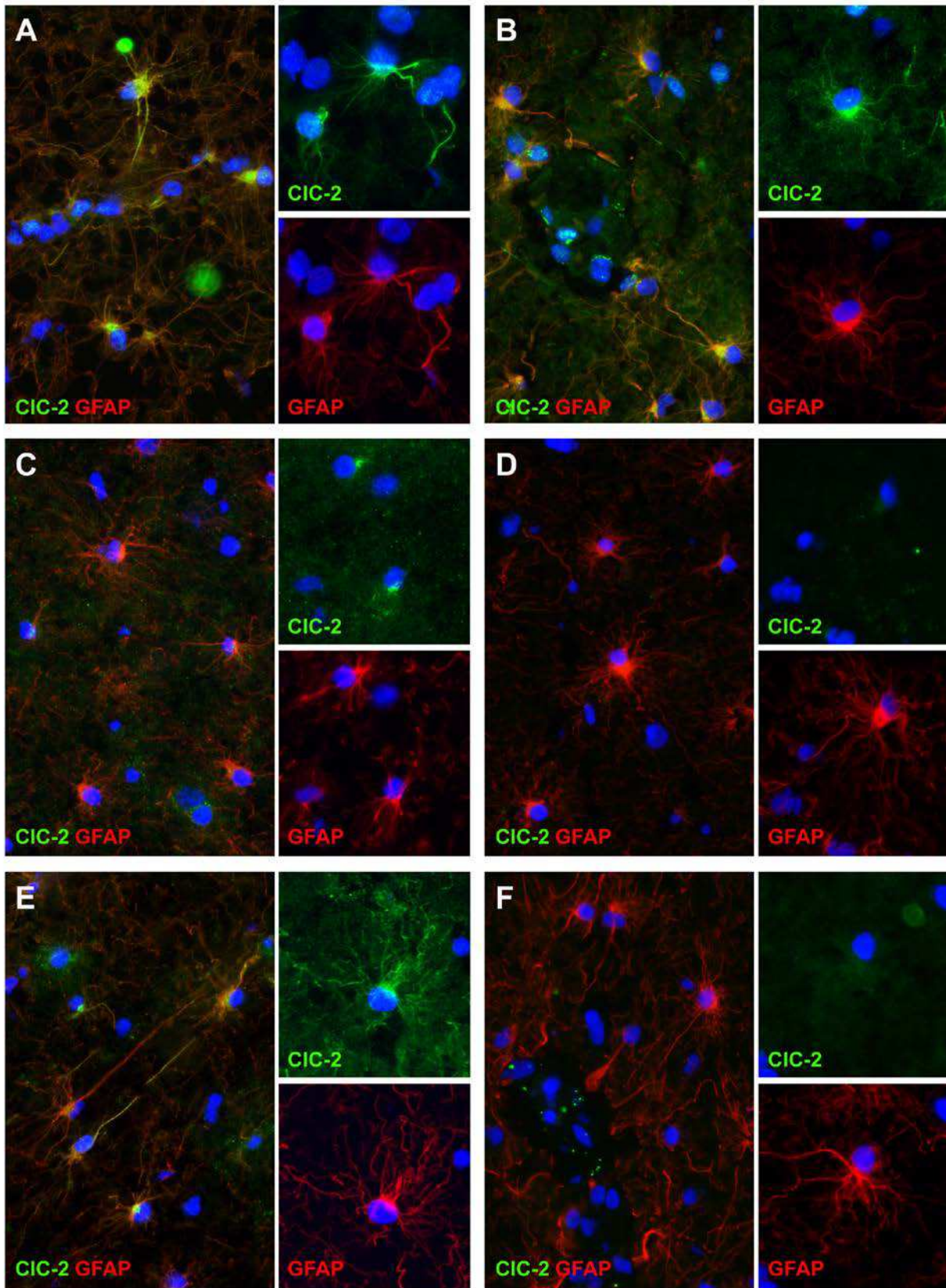
Subcellular localization of wild-type (A,C) and mutated (p.Trp570*, D,F) CIC-2 proteins, showing aberrant localization of the mutated protein in the Golgi apparatus (stained with anti-GM130, BD Biosciences 610822, 1:100, B, E). Cos7 cells were transiently transfected with wild-type or normal CIC-2-V5-His6 expression plasmid, fixed and permeabilized before staining with anti-CIC-2 (Santa Cruz SC-20122, 1:200), and examined by confocal microscopy. Scale bar: 10 μ m.

Figure S5. Validation of anti-CIC-2 antibodies in Western blot analyses



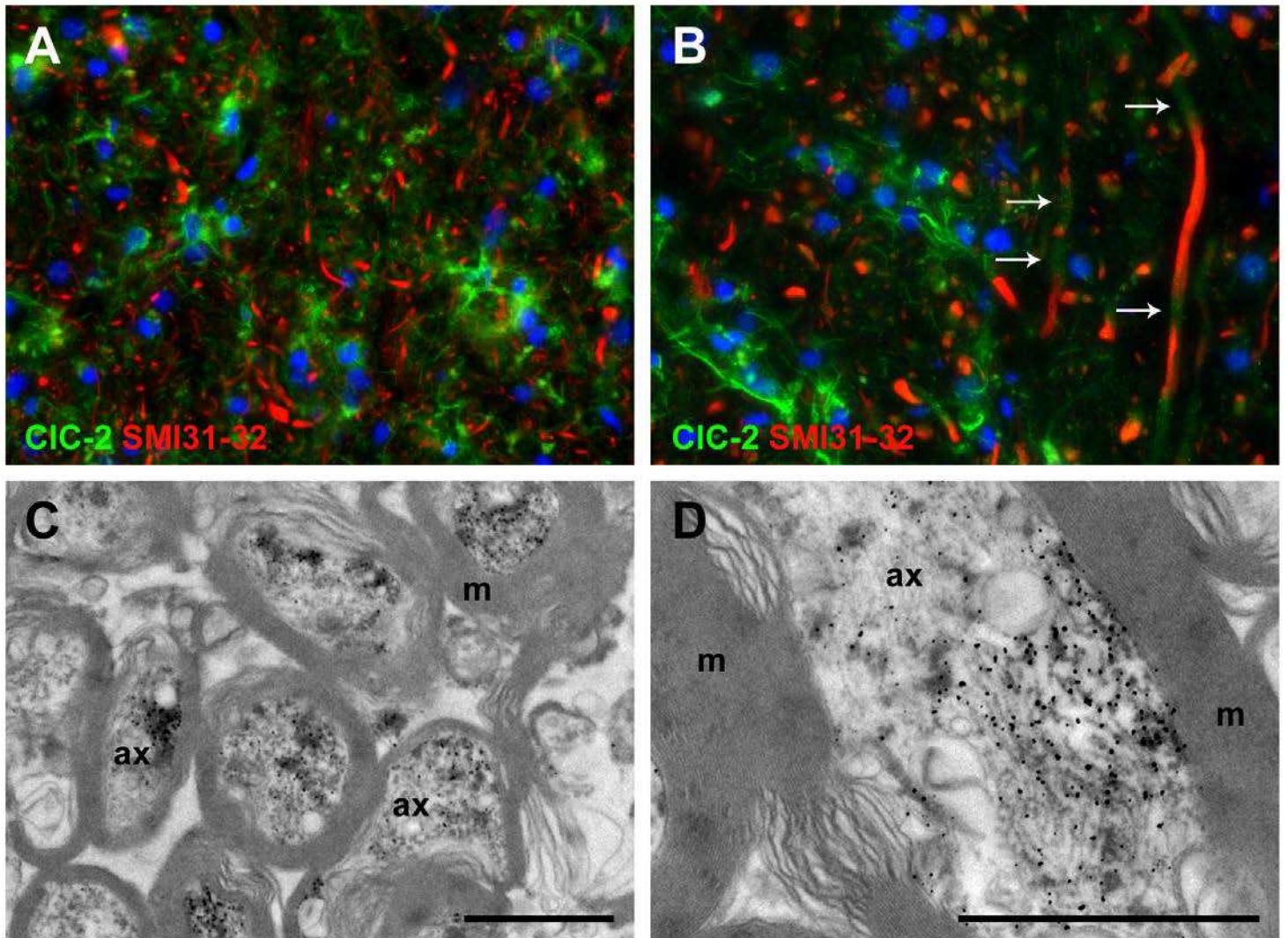
A shows the localization of the antigenic peptides that were used to raise the anti-CIC-2 antibodies. B shows Western blots of HEK293 cells after transfection with CIC-2-V5 expressing plasmids (+) or negative control (-). TCE stainings were performed to show that equal amounts of proteins were loaded. The antibodies used are indicated. C shows CIC-2 detection in control brain lysates. Only GTX113403 and SC-20122 detect a protein that migrates at the size expected for CIC-2. D shows immunocytochemistry of HEK293 cells after transfection with CIC-2-V5 expressing plasmids (+) and the negative control (-). CIC-2 was detected with the GTX113403 antibody (green). Nuclei are stained with DAPI (blue). Original magnifications: 400x.

Figure S6. Validation of the CIC-2 antibodies in fluorescent immunohistochemistry



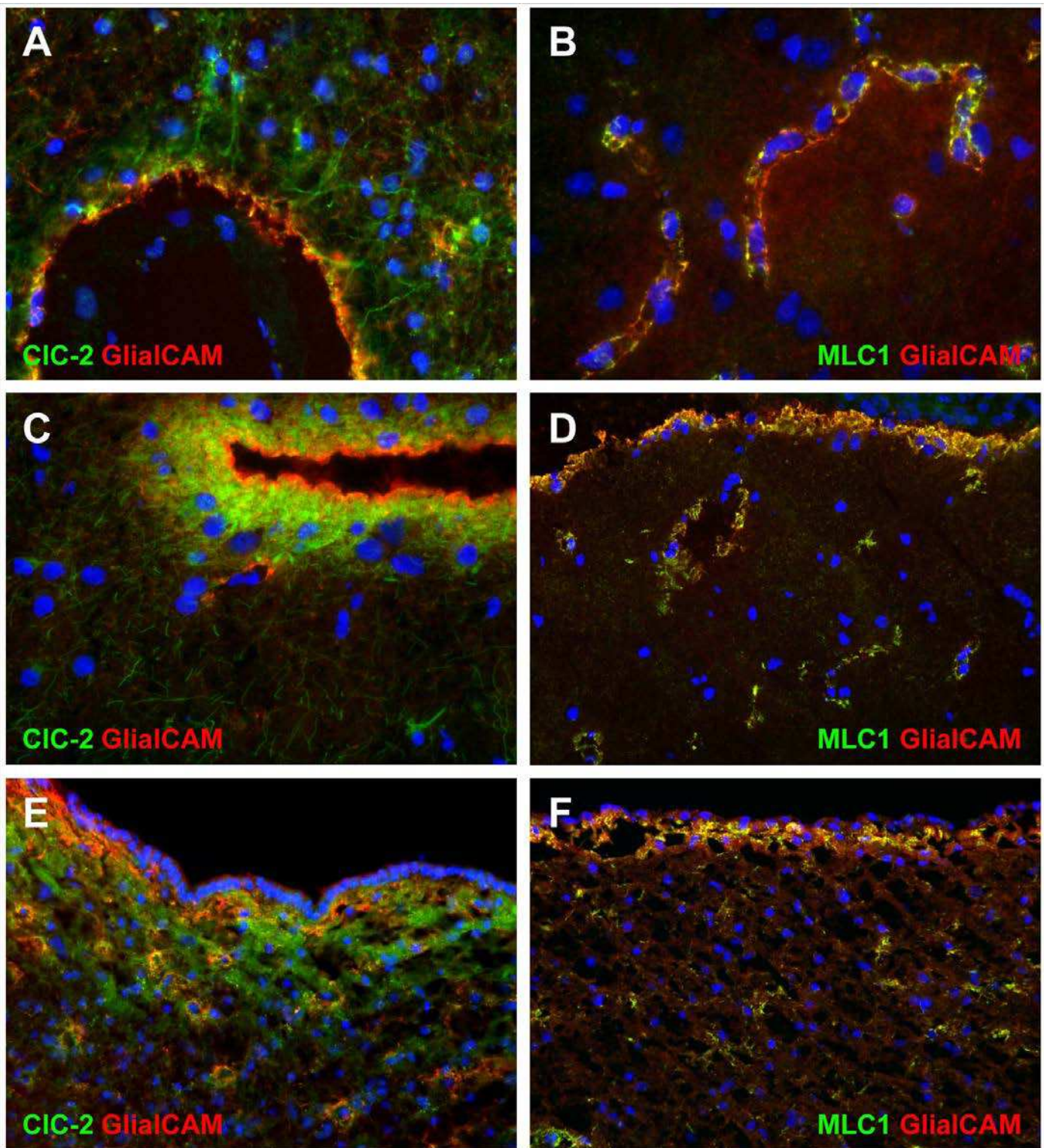
Anti-CIC-2 antibodies GTX113403 (A) and SC-20122 (B) show immunoreactivity (green) in GFAP⁺ astrocytic processes (red) in the brain, whereas HPA24108 (C) does not. A normal rabbit IgG isotype control (D) does not show immunoreactivity in astrocytes either. E and F show a blocking experiment in which the GTX113403 antibody was pre-incubated with its antigen (F) or only serum (E). Nuclei are stained with DAPI (blue). Original magnifications: 400x.

Figure S7. CIC-2 localization in axons



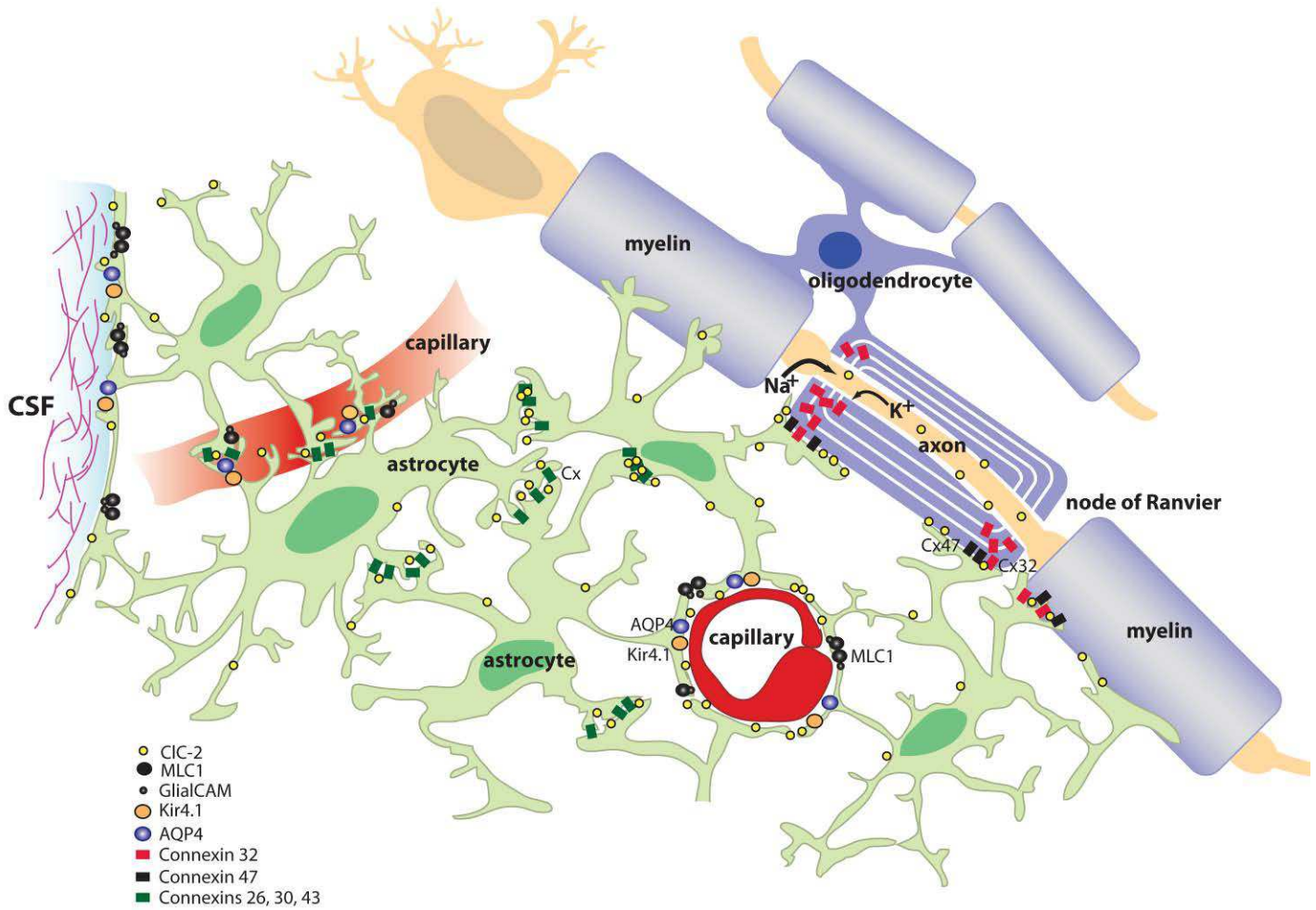
Double staining for CIC-2 (green) and the axonal markers SMI31-32 (red) of the posterior limb of the internal capsule shows numerous CIC-2⁺ astrocytes with processes abutting the surrounding axons (A, B). A fine punctate immunoreactivity is also present along the axons of larger caliber (arrows in B). Nuclei are stained with DAPI (blue). EM (C and D) confirms the presence of CIC-2 inside axons (C), associated with cytoskeletal elements and organelles, and lining the adaxonal surface of the myelin sheath (D). CIC-2 has a dynamic expression on the plasma membrane; rapid recycling and internalization could account for the abundant presence of CIC-2 in intracellular structures.⁹ Original magnifications (A, B): 400x; scale bars (C, D): 1 μm; ax: axons; m: myelin.

Figure S8. CIC-2, GlialCAM and MLC1 at blood-brain and cerebrospinal fluid-brain barriers



Double-labeling for CIC-2 and GlialCAM shows enhanced expression of CIC-2 (green) in astrocytes surrounding the blood vessels (A) and lining the surface of the brain (C) and the lateral ventricles (E). These astrocytes co-express GlialCAM (red) in the more distal portion of their cell processes and endfeet. Double staining for MLC1 (green) and GlialCAM (red) shows complete co-localization of the two proteins in the end feet of perivascular astrocytes (B), the subpial astrocytes (D), and in the ependymal cells (F). Nuclei are stained with DAPI (blue). Original magnifications: (A - C) 400x; (D - F) 200x.

Fig. S9. Schematic view of action potential-driven potassium and water fluxes



With each depolarization, sodium ions (Na^+) enter the axon at nodes of Ranvier. The compensatory exit of potassium ions (K^+) occurs at the paranodal axonal plasma membrane. K^+ and water pass through successive layers of myelin and enter the astrocytic syncytium via gap junctions, constituted by connexin32 (Cx32) and connexin47 (Cx47). The locations of CIC-2, MLC1, GlialCAM, the water channel aquaporin-4 (AQP4), the potassium channel Kir4.1 and the connexins are indicated by their respective symbols. Drawing by Dr. G.C. Scheper, modified from Rash¹⁰ and van der Knaap¹¹ with permission.

Supplementary references

1. Li H, Durbin R. Fast and accurate short read alignment with Burrows-Wheeler transform. *Bioinformatics*. **2009** Jul 15;25(14):1754-60.
2. Li H, Handsaker B, Wysoker A, et al. The Sequence Alignment/Map format and SAMtools. *Bioinformatics*. **2009** Aug 15;25(16):2078-9.
3. Saint-Martin C, Gouvain G, Teodorescu G, et al. Two novel CLCN2 mutations accelerating chloride channel deactivation are associated with idiopathic generalized epilepsy. *Hum Mutat*. **2009** Mar;30(3):397-405.
4. Scheper GC, van Berkel CG, Leisle L, et al. Analysis of CLCN2 as candidate gene for megalencephalic leukoencephalopathy with subcortical cysts. *Genet Test Mol Biomarkers*. **2010** Apr;14(2):255-7.
5. van Berge L, Kevenaar J, Polder E, et al. Pathogenic mutations causing LBSL affect mitochondrial aspartyl-tRNA synthetase in diverse ways. *Biochem J*. **2013** Mar 1;450(2):345-50.
6. Ladner CL, Yang J, Turner RJ, Edwards RA. Visible fluorescent detection of proteins in polyacrylamide gels without staining. *Anal Biochem*. **2004** Mar 1;326(1):13-20.
7. van den Pol AN, Gorcs T. Synaptic relationships between neurons containing vasopressin, gastrin-releasing peptide, vasoactive intestinal polypeptide, and glutamate decarboxylase immunoreactivity in the suprachiasmatic nucleus: dual ultrastructural immunocytochemistry with gold-substituted silver peroxidase. *J Comp Neurol*. **1986** Oct 22;252(4):507-21.
8. Dutzler R, Campbell EB, Cadene M, Chait BT, MacKinnon R. X-ray structure of a CIC chloride channel at 3.0 Å reveals the molecular basis of anion selectivity. *Nature*. **2002** Jan 17;415(6869):287-94.
9. Cornejo I, Niemeyer MI, Zuniga L, et al. Rapid recycling of CIC-2 chloride channels between plasma membrane and endosomes: role of a tyrosine endocytosis motif in surface retrieval. *J Cell Physiol*. **2009** Dec;221(3):650-7.
10. Rash JE. Molecular disruptions of the panglial syncytium block potassium siphoning and axonal saltatory conduction: pertinence to neuromyelitis optica and other demyelinating diseases of the central nervous system. *Neuroscience*. **2010** Jul 28;168(4):982-1008.
11. van der Knaap MS, Boor I, Estevez R. Megalencephalic leukoencephalopathy with subcortical cysts: chronic white matter oedema due to a defect in brain ion and water homeostasis. *Lancet Neurol*. **2012** Nov;11(11):973-85.